

Chapter 2

Fundamental Limits in Quantum Field Imaging

How Multi-Physics Correlation Extends Them

From Measurement Noise to Reconstruction Fidelity

Chapter Focus: This chapter addresses fundamental limits across the complete QFI operator stack, establishing the theoretical foundation for system design and performance prediction.

- **Measurement operator \mathcal{M} :** Quantum projection noise, sensitivity limits, resolution-sensitivity trade-off (Sections 2.2–2.3)
- **Forward model \mathcal{G} :** Conditioning, depth-resolution limits, multi-physics extension (Sections 2.4, 2.8)
- **Reconstruction operator \mathcal{R} :** Cramér-Rao bound, Γ_{inv} optimization, algorithm efficiency (Sections 2.5–2.6)
- **System-level integration:** Model-mismatch Γ_{mm} , uncertainty propagation, temporal sampling (Sections 2.7, 2.9–2.11)

QFI Pipeline Position:

$$S(\mathbf{r}) \xrightarrow{\mathcal{G}} F(\mathbf{r}) \xrightarrow{\boxed{\mathcal{M}}} D(\mathbf{r}) \xrightarrow{\mathcal{R}} \hat{S}(\mathbf{r}) \pm \sigma_S$$

Central Result: The complete QFI Imaging Figure of Merit:

$$Q_{\text{IFOM}} = Q_{\text{FOM}} \times \Gamma_{\text{inv}} \times \Gamma_{\text{mm}} \quad (\text{Central Equation})$$

Abbreviated Terms

Table 2.1: Abbreviated terms and symbols used in Chapter 2

Abbrev.	Definition	Abbrev.	Definition
<i>System Terminology</i>			
QFI	Quantum Field Imaging	QFM	Quantum Field Metrology
NV	Nitrogen-Vacancy center	ODMR	Optically Detected Magnetic Resonance
IC	Integrated Circuit	TSV	Through-Silicon Via
FA	Failure Analysis	sCMOS	Scientific CMOS
<i>Physical Quantities</i>			
QPN	Quantum Projection Noise	SQL	Standard Quantum Limit
SNR	Signal-to-Noise Ratio	FOV	Field of View
NA	Numerical Aperture	PSF	Point Spread Function
MTF	Modulation Transfer Function	ROI	Region of Interest
<i>Mathematical/Statistical</i>			
CRB	Cramér-Rao Bound	FIM	Fisher Information Matrix
MSE	Mean Squared Error	PDF	Probability Density Function
CI	Confidence Interval	UQ	Uncertainty Quantification
<i>QFI-Specific Metrics</i>			
QFOM	QFM Figure of Merit	QIFOM	QFI Imaging Figure of Merit
Γ_{inv}	Reconstruction Fidelity	Γ_{mm}	Model-Mismatch Penalty
Φ_{multi}	Multi-Physics Factor	κ	Condition Number
<i>Detector/Temporal</i>			
PRNU	Pixel Response Non-Uniformity	ROI	Region of Interest
Δt_{frame}	Frame Temporal Skew	Δt_{row}	Row Readout Time

Abstract

This chapter establishes the fundamental physical limits governing Quantum Field Imaging (QFI) systems—from measurement noise through reconstruction fidelity to final source uncertainty. Within the two-layer taxonomy that distinguishes QFM (Quantum Field Metrology: producing calibrated field maps $F(\mathbf{r})$) from QFI (Quantum Field Imaging: reconstructing source distributions $\hat{S}(\mathbf{r})$ with uncertainty bounds), we develop a comprehensive three-level limit framework:

- (1) **Measurement limits** on field estimation: quantum projection noise, the resolution-sensitivity trade-off law, and the standard quantum limit for ensemble measurements.
- (2) **Reconstruction limits** on source inference: the Cramér-Rao bound for source parameters, condition number effects on reconstruction fidelity (Γ_{inv}), and the multi-physics conditioning theorem that extends single-physics depth limits.
- (3) **System limits** on achievable accuracy: model-mismatch penalties (Γ_{mm}), calibration error budgets, temporal sampling requirements, and the complete uncertainty propagation chain from photon statistics to source confidence intervals.

The central insight is that single-physics limits, while fundamental, represent a *special case*—multi-physics correlation extends these limits by improving both information content ($\Phi_{\text{multi}} > 1$) and inverse problem conditioning ($\kappa_{\text{multi}} < \kappa_{\text{single}}$). We provide operational definitions for

all figures of merit, derive five key theorems with complete proofs, establish eight quantitative design rules, and present worked examples spanning sensitivity calculations to complete Q_{IFOM} system design.

The chapter culminates with the complete QFI Imaging Figure of Merit:

$$Q_{\text{IFOM}} = Q_{\text{FOM}} \times \Gamma_{\text{inv}} \times \Gamma_{\text{mm}}$$

which unifies measurement throughput (Q_{FOM}), reconstruction quality (Γ_{inv}), and system calibration (Γ_{mm}) into a single metric for QFI system comparison and optimization.

Chapter Roadmap (Preview)

This chapter progresses through the three-level limit framework:

Table 2.2: Chapter 2 section overview

Section	Topic	Level	Key Result
2.1	Introduction and Framework	Overview	Three-level hierarchy
2.2	Quantum Projection Noise	Level 1	Theorem 2.2.1 (SQL)
2.3	Resolution-Sensitivity Trade-off	Level 1	Theorem 2.3.1
2.4	Single-Physics Depth Limit	Level 1/2	Theorem 2.4.1
2.5	Cramér-Rao Bound	Level 2	Theorem 2.5.1 (CRB)
2.6	Γ_{inv} : Reconstruction Fidelity	Level 2	Definition, proxy formula
2.7	Γ_{mm} : Model-Mismatch	Level 3	Error budget framework
2.8	Multi-Physics Conditioning	Level 2	Theorem 2.8.1
2.9	Conditions and Failure Modes	Level 2/3	C1–C4 requirements
2.10	Uncertainty Propagation	Level 3	Complete chain
2.11	Temporal Sampling (Global Shutter)	Level 3	DR 2.8 (NEW)
2.12	Design Rules and Examples	All	DR 2.1–2.8 consolidated
2.13	How to Use This Chapter	Practical	Verification workflow
2.14	Chapter Summary	All	Q_{IFOM} synthesis

2.1 Introduction: A Three-Level Framework for Limits

2.1.1 Why This Chapter Matters

Every measurement system has fundamental limits. For QFI, these limits determine:

- The smallest magnetic field detectable (measurement limit)
- The finest spatial features resolvable (optical limit)
- The deepest buried currents reconstructible (reconstruction limit)
- The confidence with which sources can be identified (uncertainty limit)

Understanding these limits is essential for system design. But **which limits apply depends critically on whether you are doing QFM or QFI**.

The semiconductor industry faces a critical challenge: failure analysis (FA) throughput has not kept pace with transistor density growth. While Moore’s Law drives exponential increases in device complexity, FA tools remain fundamentally serial—scanning electron microscopes (SEM), focused ion beam (FIB), and scanning probe techniques all examine one point at a time. This chapter establishes the fundamental limits that constrain any imaging approach to this problem, and demonstrates how multi-physics correlation extends these limits.

2.1.2 Historical Context: From Photometry to Imaging

The distinction between measurement limits and imaging limits has deep historical roots. In optical astronomy, photometric sensitivity (measuring stellar brightness) improved steadily for centuries. However, the ability to *image* faint sources required solving an inverse problem: deconvolving atmospheric turbulence, optical aberrations, and detector noise from the true source distribution.

The introduction of CCDs in the 1970s revolutionized astronomy not merely by improving sensitivity, but by enabling parallel photon integration across many pixels simultaneously—the entire field was captured in a single exposure rather than scanned point-by-point.

However, CCD readout remained sequential (the “bucket brigade” architecture), introducing temporal skew between first and last pixels read. Modern scientific CMOS (sCMOS) sensors offer two distinct readout modes with profound implications for QFI:

Readout Mode	Mechanism	QFI Implications
Rolling Shutter	Rows exposed and read sequentially; temporal skew $\Delta t = N_{\text{rows}} \times t_{\text{row}}$	Creates time-smeared field map; invalid for dynamic phenomena
Global Shutter	All pixels integrate simultaneously, then read sequentially	True instantaneous snapshot; essential for time-resolved QFI

Table 2.3: Comparison of sCMOS readout modes for QFI applications

Design Rule: Global Shutter Requirement for Dynamic QFI

For QFI of dynamic phenomena—magnetic domain walls moving at ~ 100 m/s, thermal transients with \sim ms timescales, or time-resolved strain—global shutter is not merely preferable but essential. The temporal skew of rolling shutter corrupts spatial correlations and invalidates the instantaneous field assumption underlying the QFI forward model.

Quantitative criterion: Global shutter required when:

$$v_{\text{feature}} \times t_{\text{rolling}} > \delta x_{\text{target}} \quad (2.1)$$

where v_{feature} is the feature velocity, t_{rolling} is the rolling shutter sweep time, and δx_{target} is the target spatial resolution.

Example 2.1.1 (Rolling vs. Global Shutter for Magnetic Domain Imaging). Consider imaging magnetic domain walls moving at $v = 100$ m/s with a 1024×1024 sCMOS sensor having row readout time $t_{\text{row}} = 10 \mu\text{s}$:

- Rolling shutter sweep time: $t_{\text{rolling}} = 1024 \times 10 \mu\text{s} = 10.24 \text{ ms}$
- Domain wall displacement during readout: $\Delta x = 100 \text{ m/s} \times 10.24 \text{ ms} = 1.024 \text{ m} \approx 1 \text{ mm}$
- For target resolution $\delta x = 1 \mu\text{m}$: rolling shutter displacement exceeds target by factor 10^3

Conclusion: Global shutter mandatory for dynamic magnetic imaging at micron resolution.

QFI represents an analogous revolution: the transition from serial quantum sensing (high sensitivity, single-point) to parallel quantum measurement (field maps) and ultimately to source reconstruction (imaging). This chapter establishes which limits constrain each level.

2.1.3 The Three-Level Limit Hierarchy

The Limit Hierarchy

QFI systems face three distinct levels of fundamental limits:

1. **Measurement limits (\mathcal{M} operator):** Quantum projection noise, shot noise, sensitivity floor—these constrain the field map $F(\mathbf{r})$
2. **Reconstruction limits (\mathcal{R} operator):** Cramér-Rao bound, conditioning, regularization—these constrain the source estimate $\hat{S}(\mathbf{r})$
3. **System limits (\mathcal{G} - \mathcal{M} - \mathcal{R} chain):** Model-mismatch, calibration errors, drift—these degrade achievable accuracy below theoretical limits

A QFM system is bounded by Level 1 only. A QFI system must satisfy all three.

Level	Limit Type	Governs	Key Metric
1	Measurement (\mathcal{M})	Field uncertainty σ_F	Q_{FOM}
2	Reconstruction (\mathcal{R})	Source uncertainty σ_S	Γ_{inv}
3	System (\mathcal{G} - \mathcal{M} - \mathcal{R})	Achievable accuracy	Γ_{mm}

Table 2.4: Three-level limit hierarchy for QFI systems

The three-level hierarchy reflects the QFI operator stack:

$$S(\mathbf{r}) \xrightarrow{\mathcal{G}} F(\mathbf{r}) \xrightarrow{\mathcal{M}} D \xrightarrow{\mathcal{R}} \hat{S}(\mathbf{r}) \quad (2.2)$$

Level 1 limits govern the \mathcal{M} operator (how well we measure the field). Level 2 limits govern the \mathcal{R} operator (how well we reconstruct sources from measurements). Level 3 limits govern the entire chain (how well our model matches reality).

2.1.4 QFM vs. QFI: Different Limits Apply

The distinction between QFM and QFI is not merely semantic—it determines which fundamental limits apply and what figures of merit are appropriate.

Aspect	QFM (Metrology)	QFI (Imaging)
Output	Field map $F(\mathbf{r})$	Source estimate $\hat{S}(\mathbf{r}) \pm \sigma_S$
Fundamental limit	$\sigma_F \geq \sigma_F^{\text{SQL}}$	$\sigma_S \geq \sqrt{\text{CRB}}$
Limiting operator	\mathcal{M} only	$\mathcal{G} + \mathcal{M} + \mathcal{R}$ (complete stack)
Figure of merit	Q_{FOM}	$Q_{\text{IFOM}} = Q_{\text{FOM}} \times \Gamma_{\text{inv}} \times \Gamma_{\text{mm}}$
Improvable by algorithm?	No (physics limit)	Partially (\mathcal{R} optimization)

Table 2.5: Different limits apply to QFM vs. QFI systems

Definition 2.1.1 (Standard Quantum Limit for Field Measurement). The Standard Quantum Limit (SQL) for magnetic field measurement using N independent quantum sensors with coherence time T_2 is:

$$\sigma_B^{\text{SQL}} = \frac{1}{\gamma \sqrt{NT_2 t}} \quad (2.3)$$

where γ is the gyromagnetic ratio and t is the total measurement time. This represents Level 1—the fundamental measurement limit.

Definition 2.1.2 (Cramér-Rao Bound for Source Reconstruction). The Cramér-Rao Bound (CRB) provides the minimum achievable variance for any unbiased estimator of source parameters \mathbf{S} :

$$\text{Cov}(\hat{\mathbf{S}}) \geq \mathbf{J}^{-1} \quad (2.4)$$

where \mathbf{J} is the Fisher Information Matrix. This represents Level 2—the fundamental reconstruction limit.

2.1.5 Pain Points in Current Semiconductor Metrology

The semiconductor industry faces specific challenges that motivate the QFI approach:

Pain Point	Current Limitation	Impact	QFI Solution
Throughput	Serial scanning: point/ms	1 Day per die	Parallel: points $10^4\text{--}10^6$
Depth access	Surface-only or destructive	Miss buried defects	Non-invasive depth reconstruction
Physics ambiguity	Single-physics (thermal only)	Cannot identify root cause	Multi-physics correlation
Quantification	Qualitative “hot spot”	No current values	Quantitative $I(\mathbf{r}) \pm \sigma_I$

Table 2.6: Pain points in semiconductor FA and QFI solutions

2.1.6 Figures of Merit for This Chapter

This chapter establishes quantitative figures of merit for each limit level:

FOM	Symbol	Definition	Target Value
Field sensitivity	σ_B	Minimum detectable field	$< 1 \text{ nT}/\sqrt{\text{Hz}}$
Spatial resolution	δx	FWHM of PSF	$< 1 \mu\text{m}$
Reconstruction fidelity	Γ_{inv}	CRB/MSE	> 0.7
Model-mismatch penalty	Γ_{mm}	$\prod(1 - \epsilon_i^2)$	> 0.9
Imaging FOM	Q_{IFOM}	$Q_{\text{FOM}} \times \Gamma_{\text{inv}} \times \Gamma_{\text{mm}}$	$> 10^8 \text{ px/s}$
Depth limit	z_{max}	Maximum reconstructible depth	$> 50 \mu\text{m}$
Condition number	κ	$\sigma_{\text{max}}/\sigma_{\text{min}}$ of \mathbf{G}	< 100

Table 2.7: Key figures of merit established in Chapter 2

2.1.7 Chapter Roadmap

This chapter progresses through the three limit levels:

1. **Sections 2.2–2.3:** Measurement limits (quantum projection noise, resolution-sensitivity trade-off)—Level 1
2. **Section 2.4:** Single-physics depth limit (baseline for magnetic-only reconstruction)
3. **Section 2.5:** Cramér-Rao bound for source parameters—Level 2
4. **Section 2.6:** Γ_{inv} —reconstruction fidelity factor
5. **Section 2.7:** Γ_{mm} —model-mismatch framework—Level 3
6. **Section 2.8:** Multi-physics conditioning theorem (how multi-physics extends limits)

7. **Section 2.9:** Failure modes and diagnostic strategies
8. **Section 2.10:** Complete uncertainty propagation chain
9. **Section 2.11:** Global shutter design rules for dynamic QFI
10. **Section 2.12:** Consolidated design rules
11. **Sections 2.13–2.14:** Verification workflow and chapter summary

By the end of this chapter, readers will understand not only what limits exist, but how to quantify them, how to design systems that approach them, and how multi-physics correlation extends single-physics baselines.

2.2 Quantum Projection Noise: The Measurement Floor

2.2.1 Physical Origin of Quantum Projection Noise

Quantum Projection Noise (QPN) represents the fundamental uncertainty in measuring quantum states. For NV center-based QFI, QPN arises from the statistical nature of spin state projection during optical readout.

Consider an ensemble of N NV centers prepared in a superposition state:

$$|\psi\rangle = \cos(\theta/2)|0\rangle + \sin(\theta/2)|1\rangle \quad (2.5)$$

where the angle θ encodes the magnetic field through the phase accumulated during free precession: $\theta = \gamma B \tau$, with γ the gyromagnetic ratio and τ the sensing time.

Upon measurement, each NV center projects to either $|0\rangle$ or $|1\rangle$ with probabilities $p_0 = \cos^2(\theta/2)$ and $p_1 = \sin^2(\theta/2)$. The number of NV centers measured in state $|0\rangle$ follows a binomial distribution:

$$\langle n_0 \rangle = N p_0, \quad \sigma_{n_0} = \sqrt{N p_0 (1 - p_0)} \quad (2.6)$$

The signal (change in n_0 per unit field) is:

$$\frac{\partial n_0}{\partial B} = -N \gamma \tau \sin(\theta) \quad (2.7)$$

Maximum sensitivity occurs at $\theta = \pi/2$ (half-way point of Ramsey fringe), where $\sin(\theta) = 1$ and $p_0 = p_1 = 1/2$, giving $\sigma_{n_0} = \sqrt{N}/2$.

2.2.2 Derivation of the QPN Limit

Theorem 2.2.1 (Quantum Projection Noise Limit). *For an ensemble of N independent NV centers with readout contrast C and photon collection efficiency η , the minimum detectable magnetic field uncertainty is:*

$$\sigma_B^{\text{QPN}} = \frac{1}{C \gamma \sqrt{N \eta}} \cdot \frac{1}{\sqrt{\tau}} \quad (2.8)$$

where τ is the coherent sensing time per measurement cycle.

Proof. Starting from the error propagation:

$$\sigma_B = \frac{\sigma_{n_0}}{|\partial n_0 / \partial B|} = \frac{\sqrt{N p_0 (1 - p_0)}}{N C \gamma \tau} \quad (2.9)$$

At optimal working point ($\theta = \pi/2$, $p_0 = 1/2$):

$$\sigma_B = \frac{\sqrt{N/4}}{N C \gamma \tau} = \frac{1}{2 C \gamma \sqrt{N} \tau} \quad (2.10)$$

Including photon collection efficiency η (which effectively reduces the number of detected photons):

$$\sigma_B^{\text{QPN}} = \frac{1}{C\gamma\sqrt{N\eta\tau}} \quad (2.11)$$

For measurement time t with duty cycle approaching unity (continuous sensing):

$$\sigma_B^{\text{QPN}} = \frac{1}{C\gamma\sqrt{N\eta}} \cdot \frac{1}{\sqrt{t}} \quad (2.12)$$

□

Key Equation: Sensitivity Figure of Merit

The magnetic field sensitivity (in $\text{T}/\sqrt{\text{Hz}}$) for QFI is:

$$\boxed{\eta_B = \frac{1}{C\gamma\sqrt{N\eta T_2^*}}} \quad (2.13)$$

where T_2^* is the dephasing time that limits coherent sensing duration.

2.2.3 Numerical Analysis of QPN Scaling

Example 2.2.1 (QPN Limit for Typical QFI Parameters). Consider a QFI system with:

- NV density: $\rho_{\text{NV}} = 1 \times 10^{17} \text{ cm}^{-3}$
- Diamond layer thickness: $d = 100 \text{ nm}$
- Pixel area: $A_{\text{pix}} = 1 \mu\text{m} \times 1 \mu\text{m}$
- Readout contrast: $C = 0.3$
- Collection efficiency: $\eta = 0.1$
- Gyromagnetic ratio: $\gamma = 28 \text{ GHz/T}$
- Dephasing time: $T_2^* = 1 \mu\text{s}$

Step 1: Calculate NV count per pixel

$$N = \rho_{\text{NV}} \times d \times A_{\text{pix}} = 10^{17} \times 10^{-5} \times 10^{-8} = 10^4 \text{ NV centers} \quad (2.14)$$

Step 2: Calculate sensitivity

$$\eta_B = \frac{1}{C\gamma\sqrt{N\eta T_2^*}} \quad (2.15)$$

$$= \frac{1}{0.3 \times 2.8 \times 10^{10} \times \sqrt{10^4 \times 0.1 \times 10^{-6}}} \quad (2.16)$$

$$= \frac{1}{8.4 \times 10^9 \times \sqrt{10^{-3}}} \quad (2.17)$$

$$= \frac{1}{8.4 \times 10^9 \times 0.0316} \quad (2.18)$$

$$= 3.8 \times 10^{-9} \text{ T}/\sqrt{\text{Hz}} = 3.8 \text{ nT}/\sqrt{\text{Hz}} \quad (2.19)$$

Result: Single-pixel sensitivity $\eta_B \approx 4 \text{ nT}/\sqrt{\text{Hz}}$

Step 3: For 1-second integration

$$\sigma_B = \eta_B/\sqrt{t} = 3.8 \text{ nT}/\sqrt{1 \text{ s}} = 3.8 \text{ nT} \quad (2.20)$$

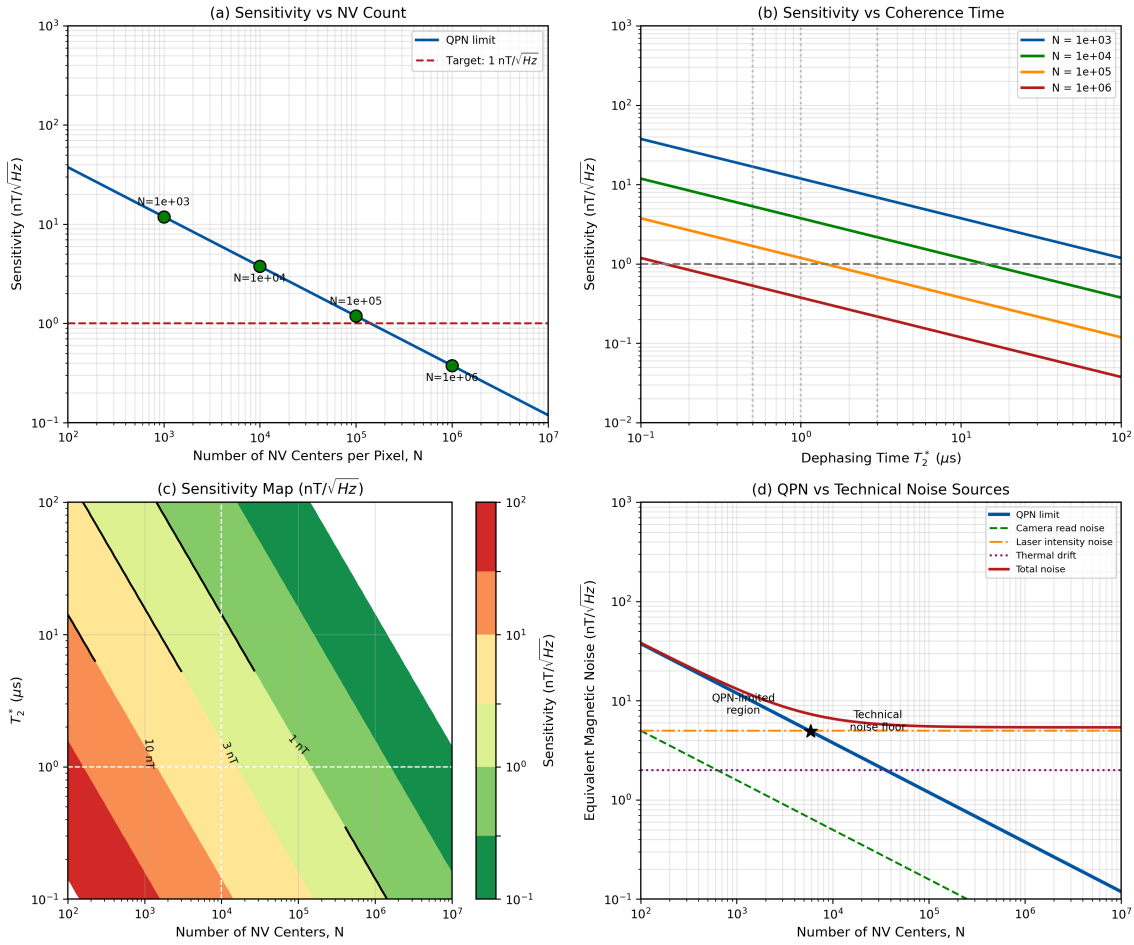


Figure 2.1: Quantum Projection Noise scaling analysis. (a) Sensitivity vs. NV count showing $1/\sqrt{N}$ scaling; horizontal dashed line indicates $1 \text{nT}/\sqrt{\text{Hz}}$ target. (b) Sensitivity vs. dephasing time T_2^* for different NV densities; longer coherence enables better sensitivity. (c) Sensitivity map as function of both N and T_2^* with contours at 1, 3, and $10 \text{nT}/\sqrt{\text{Hz}}$. (d) Comparison of QPN limit with technical noise sources showing crossover points. **Parameters:** $C = 0.3$, $\eta = 0.1$, $\gamma = 28 \text{ GHz/T}$.

2.2.4 Factors Affecting QPN Performance

Parameter	Symbol	Typical Range	Scaling Impact
NV count	N	$10^3\text{--}10^6$	$\sigma_B \propto 1/\sqrt{N}$
Contrast	C	0.1–0.4	$\sigma_B \propto 1/C$
Collection efficiency	η	0.01–0.2	$\sigma_B \propto 1/\sqrt{\eta}$
Dephasing time	T_2^*	0.1–10 μs	$\sigma_B \propto 1/\sqrt{T_2^*}$
Measurement time	t	1 ms–10 s	$\sigma_B \propto 1/\sqrt{t}$

Table 2.8: Parameters affecting QPN-limited sensitivity

For sub-nT sensitivity in QFI applications:

1. **NV count:** Target $N > 10^5$ per pixel (achievable with $\rho_{\text{NV}} > 10^{17} \text{ cm}^{-3}$ and $1 \mu\text{m}$ pixels)
 2. **Contrast:** Optimize pulse sequences for $C > 0.25$; consider charge state preparation
 3. **Collection:** Design optics for $\eta > 0.1$; high-NA objectives essential
 4. **Coherence:** Use isotopically purified ^{12}C diamond for $T_2^* > 1 \mu\text{s}$
- Target sensitivity:** $\eta_B < 1 \text{ nT}/\sqrt{\text{Hz}}$ requires $N\eta T_2^* C^2 > 10^{-3} \text{ s}$.

2.2.5 QPN and the Standard Quantum Limit

The QPN limit represents the Standard Quantum Limit (SQL) for independent quantum sensors. This is a Level 1 limit that cannot be exceeded without:

- Quantum entanglement between sensors (Heisenberg scaling: $\sigma_B \propto 1/N$)
- Squeezed states (up to \sqrt{N} improvement)
- Quantum error correction (extending effective T_2^*)

Warning: SQL is a Measurement Limit, Not an Imaging Limit

The SQL constrains the field measurement σ_F , not the source reconstruction σ_S . A system can achieve SQL-limited field measurement but still have poor imaging performance due to ill-conditioned reconstruction. This distinction between Level 1 and Level 2 limits is central to the QFI framework.

2.2.6 From Field Sensitivity to Imaging Performance

The connection between QPN-limited field sensitivity and imaging performance involves the entire operator stack:

$$\sigma_S^2 = \left(\frac{\partial S}{\partial F} \right)^2 \sigma_F^2 = \mathbf{G}^{-1} \cdot \sigma_F^2 \cdot (\mathbf{G}^{-1})^T \quad (2.21)$$

For ill-conditioned forward models \mathbf{G} , small field uncertainties σ_F can amplify into large source uncertainties σ_S . This amplification is quantified by the condition number $\kappa = \sigma_{\max}/\sigma_{\min}$ of \mathbf{G} , which we examine in Section 2.5.

2.3 Resolution-Sensitivity Trade-off

2.3.1 The Fundamental Trade-off

In QFI systems, there exists a fundamental trade-off between spatial resolution and magnetic field sensitivity. This trade-off arises because improving resolution (smaller pixels) reduces the number of NV centers per pixel, thereby degrading sensitivity.

Theorem 2.3.1 (Resolution-Sensitivity Trade-off). *For a QFI system with fixed NV layer properties, the product of spatial resolution δx and magnetic field sensitivity σ_B satisfies:*

$$\sigma_B \cdot \delta x \geq \frac{\text{const}}{\sqrt{\rho_{\text{NV}} d \cdot \eta C^2 \gamma^2 T_2^*}} \quad (2.22)$$

where ρ_{NV} is the NV density, d is the NV layer thickness, η is collection efficiency, C is contrast, γ is gyromagnetic ratio, and T_2^* is the dephasing time.

Proof. For pixel size δx , the number of NV centers per pixel is:

$$N = \rho_{\text{NV}} \cdot d \cdot (\delta x)^2 \quad (2.23)$$

Substituting into the QPN sensitivity formula:

$$\sigma_B = \frac{1}{C\gamma\sqrt{N\eta T_2^*}} \quad (2.24)$$

$$= \frac{1}{C\gamma\sqrt{\rho_{\text{NV}}d \cdot \eta T_2^*}} \cdot \frac{1}{\delta x} \quad (2.25)$$

Therefore:

$$\sigma_B \cdot \delta x = \frac{1}{C\gamma\sqrt{\rho_{\text{NV}}d \cdot \eta T_2^*}} = \text{const} \quad (2.26)$$

The equality holds when operating at the QPN limit; technical noise raises this floor. \square

Key Equation: Trade-off Constant

The resolution-sensitivity product constant K is:

$$K = \sigma_B \cdot \delta x = \frac{1}{C\gamma\sqrt{\rho_{\text{NV}}d \cdot \eta T_2^*}} \quad (2.27)$$

Lower K indicates better trade-off (simultaneously achievable resolution and sensitivity). Typical values: $K = 10\text{--}100 \text{ nT}\cdot\mu\text{m}/\sqrt{\text{Hz}}$.

2.3.2 Numerical Example: Trade-off Constant Calculation

Example 2.3.1 (Calculating the Trade-off Constant). For a typical QFI system:

- NV density: $\rho_{\text{NV}} = 10^{17} \text{ cm}^{-3} = 10^{23} \text{ m}^{-3}$
- Layer thickness: $d = 100 \text{ nm} = 10^{-7} \text{ m}$
- Collection efficiency: $\eta = 0.1$
- Contrast: $C = 0.3$
- Dephasing time: $T_2^* = 1 \mu\text{s} = 10^{-6} \text{ s}$
- Gyromagnetic ratio: $\gamma = 2.8 \times 10^{10} \text{ Hz/T}$

Calculate the volume density-thickness product:

$$\rho_{\text{NV}} \cdot d = 10^{23} \times 10^{-7} = 10^{16} \text{ m}^{-2} \quad (2.28)$$

Calculate K :

$$K = \frac{1}{0.3 \times 2.8 \times 10^{10} \times \sqrt{10^{16} \times 0.1 \times 10^{-6}}} \quad (2.29)$$

$$= \frac{1}{8.4 \times 10^9 \times \sqrt{10^9}} \quad (2.30)$$

$$= \frac{1}{8.4 \times 10^9 \times 3.16 \times 10^4} \quad (2.31)$$

$$= \frac{1}{2.65 \times 10^{14}} \quad (2.32)$$

$$= 3.8 \times 10^{-15} \text{ T} \cdot \text{m}/\sqrt{\text{Hz}} \quad (2.33)$$

Convert to practical units:

$$K = 3.8 \times 10^{-15} \text{ T} \cdot \text{m}/\sqrt{\text{Hz}} = 3.8 \text{ nT} \cdot \mu\text{m}/\sqrt{\text{Hz}} \quad (2.34)$$

Interpretation: With this K value:

- At $\delta x = 1 \mu\text{m}$: $\sigma_B = 3.8 \text{ nT}/\sqrt{\text{Hz}}$
- At $\delta x = 0.5 \mu\text{m}$: $\sigma_B = 7.6 \text{ nT}/\sqrt{\text{Hz}}$
- At $\sigma_B = 1 \text{ nT}/\sqrt{\text{Hz}}$: $\delta x = 3.8 \mu\text{m}$

2.3.3 Trade-off Curves and Operating Regions

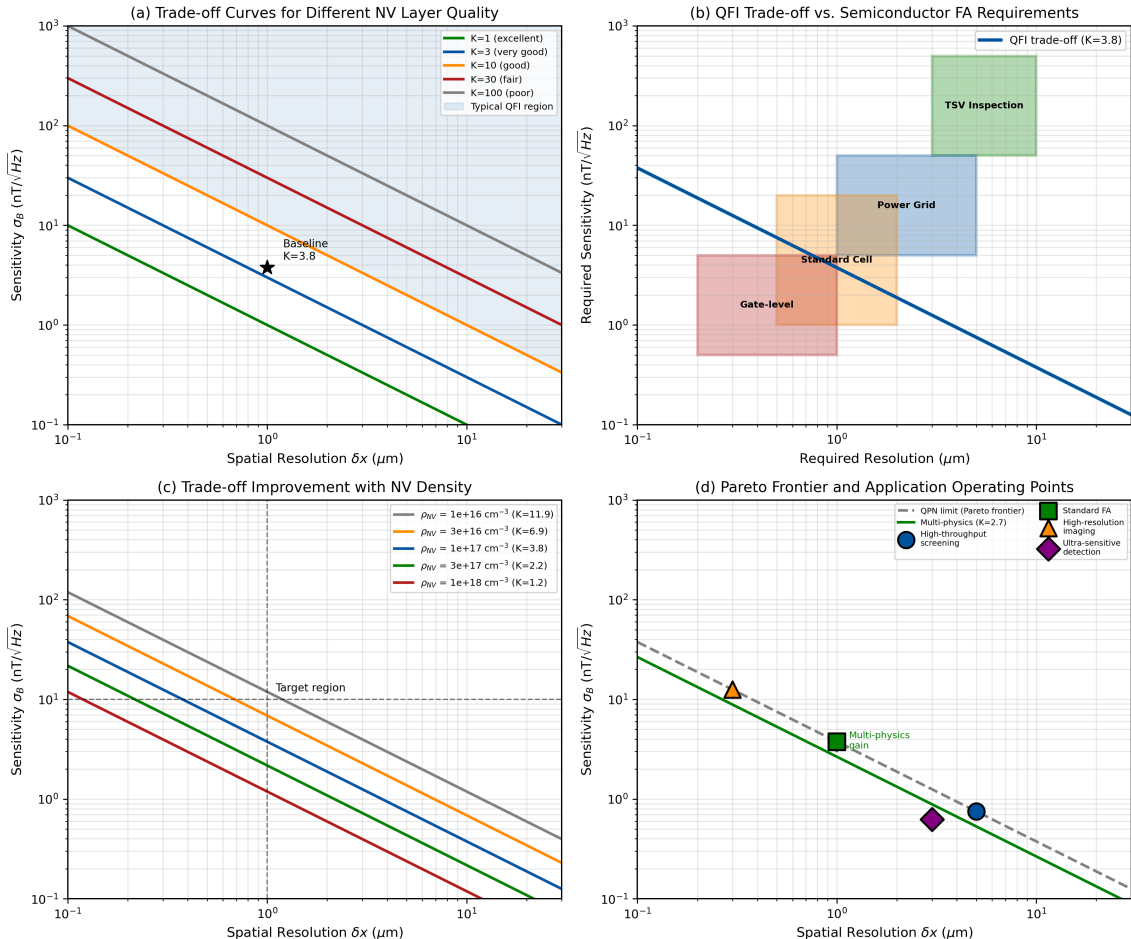


Figure 2.2: Resolution-sensitivity trade-off analysis. (a) Trade-off curves for different NV layer qualities (different K values); shaded regions indicate practically achievable combinations. (b) Comparison with semiconductor FA requirements; intersection defines viable QFI operating region. (c) Effect of NV density on trade-off constant; higher density shifts curve toward better performance. (d) Pareto frontier showing optimal operating points for different applications. **Parameters:** Baseline $\rho_{\text{NV}} = 10^{17} \text{ cm}^{-3}$, $d = 100 \text{ nm}$, $\eta = 0.1$, $C = 0.3$, $T_2^* = 1 \mu\text{s}$.

2.3.4 Strategies to Improve the Trade-off

The trade-off constant K can be reduced (improved) by:

Strategy	Parameter	Practical Approach	Improvement Factor
Increase NV density	$\rho_{\text{NV}} \uparrow$	High-dose implantation, optimized annealing	2–5×
Thicker NV layer	$d \uparrow$	Epitaxial growth, CVD layers	2–3×
Better collection	$\eta \uparrow$	High-NA optics, SIL	3–10×
Higher contrast	$C \uparrow$	Charge state prep, optimized sequences	1.5–2×
Longer coherence	$T_2^* \uparrow$	^{12}C purification, dynamical decoupling	3–10×

Table 2.9: Strategies for improving the resolution-sensitivity trade-off

2.3.5 Comparison with Semiconductor FA Requirements

Application	Resolution	Sensitivity	Required K	Status
TSV inspection	5 μm	100 nT	500 nT· μm	Achievable
Power grid mapping	2 μm	10 nT	20 nT· μm	Achievable
Standard cell FA	1 μm	5 nT	5 nT· μm	Challenging
Gate-level FA	0.5 μm	1 nT	0.5 nT· μm	R&D frontier

Table 2.10: Resolution-sensitivity requirements for semiconductor FA applications

Design Rule: Trade-off Budget Allocation

For QFI system design, allocate the trade-off budget based on application priority:

1. **Resolution-critical** (gate-level FA): Prioritize smaller δx , accept higher σ_B , use longer integration
2. **Sensitivity-critical** (weak defect detection): Prioritize lower σ_B , accept larger δx , use binning
3. **Balanced** (typical FA): Target $K < 10 \text{ nT}\cdot\mu\text{m}/\sqrt{\text{Hz}}$

Quantitative guideline: For standard cell FA at 7 nm node, target $\delta x < 1 \mu\text{m}$ and $\sigma_B < 10 \text{ nT}/\sqrt{\text{Hz}}$, requiring $K < 10 \text{ nT}\cdot\mu\text{m}/\sqrt{\text{Hz}}$.

2.3.6 Breaking the Trade-off with Multi-Physics

The resolution-sensitivity trade-off derived above applies to *single-physics* (magnetic-only) measurement. Multi-physics correlation can effectively break this trade-off by:

1. **Information fusion:** Combining magnetic and thermal measurements provides complementary information that improves effective sensitivity without sacrificing resolution
2. **Regularization:** Multi-physics data constrains the inverse problem, improving Γ_{inv} and effectively lowering σ_S for the same σ_F
3. **Systematic error cancellation:** Correlated systematic errors (e.g., standoff distance uncertainty) partially cancel in multi-physics ratios

Multi-Physics Extends the Trade-off

While the QPN-limited trade-off (Equation 2.22) is fundamental for single-physics measurement, multi-physics correlation extends this limit by improving reconstruction fidelity Γ_{inv} . The effective trade-off becomes:

$$\sigma_S \cdot \delta x \geq \frac{K}{\sqrt{\Phi_{\text{multi}}}} \cdot \frac{1}{\sqrt{\Gamma_{\text{inv}}}} \quad (2.35)$$

where $\Phi_{\text{multi}} > 1$ is the multi-physics information gain and Γ_{inv} improves with better conditioning. This is a Level 2 effect, distinct from the Level 1 measurement trade-off.

2.3.7 Practical Design Considerations

When designing a QFI system, the resolution-sensitivity trade-off must be considered alongside other constraints:

1. **Field of view vs. resolution:** Larger FOV at fixed pixel count means larger pixels, better sensitivity, but worse resolution
2. **Frame rate vs. sensitivity:** Faster frame rates mean less integration time per frame, degrading sensitivity
3. **Dynamic range:** Very high sensitivity may saturate on strong sources; design for the expected field range

Example 2.3.2 (System Design Trade-off). Design a QFI system for IC failure analysis with:

- Target: Map $100 \times 100 \mu\text{m}^2$ area with $1 \mu\text{m}$ resolution
- Camera: 1024×1024 pixels
- Required pixel size: $100 \mu\text{m} / 1024 \approx 0.1 \mu\text{m}$ at sample (but target $1 \mu\text{m}$ resolution, so $10 \times$ binning possible)

Option A: Native $1 \mu\text{m}$ pixels (no binning)

- $N = 10^4 \text{ NV/pixel} \rightarrow \sigma_B \approx 4 \text{ nT}/\sqrt{\text{Hz}}$
- Meets standard cell FA requirement

Option B: $0.5 \mu\text{m}$ pixels with 2×2 binning for dynamic mode

- High-res mode: $N = 2.5 \times 10^3 \text{ NV/pixel} \rightarrow \sigma_B \approx 8 \text{ nT}/\sqrt{\text{Hz}}$
- Binned mode: $N = 10^4 \text{ NV/pixel} \rightarrow \sigma_B \approx 4 \text{ nT}/\sqrt{\text{Hz}}$
- Flexible for different FA scenarios

Recommendation: Option B provides flexibility for both high-resolution structural imaging and high-sensitivity defect detection.

2.4 Single-Physics Depth Limit: The Baseline Constraint

2.4.1 Physical Origin of Depth-Resolution Coupling

For magnetic-only QFI, the ability to resolve lateral features degrades with source depth. This fundamental constraint arises from the physics of static magnetic field propagation: the Biot-Savart law dictates that high spatial frequencies (fine features) in the source current attenuate exponentially with distance.

Consider a current source at depth z with spatial frequency content up to wavenumber k . The magnetic field at the surface can be expressed in Fourier space:

$$\tilde{B}(k_x, k_y, z = 0) = \tilde{G}(k_x, k_y, z) \cdot \tilde{J}(k_x, k_y) \quad (2.36)$$

where the Green's function transfer behaves as:

$$|\tilde{G}(k, z)| \propto e^{-|k|z} \quad (2.37)$$

This exponential attenuation means that for a source at depth z :

- Features smaller than $\sim z$ are exponentially suppressed
- The effective low-pass filter cutoff is $k_c \sim 1/z$
- Information about fine structure is lost before it reaches the sensor

2.4.2 The Depth Theorem

Theorem 2.4.1 (Single-Physics Depth Limit). *For magnetic-only QFI, the minimum resolvable feature size δx_{\min} at depth z is bounded by:*

$$\boxed{\delta x_{\min} \geq \frac{z}{\sqrt{\text{SNR}}}} \quad (2.38)$$

where SNR is the signal-to-noise ratio at the measurement plane. This represents a fundamental single-physics baseline that multi-physics correlation can extend.

Proof. From the exponential decay of high spatial frequencies (Equation 2.37), a feature of size δx at depth z produces surface field with amplitude:

$$B_{\text{surface}} \sim B_0 \cdot e^{-2\pi z/\delta x} \quad (2.39)$$

For detectability, we require $B_{\text{surface}} > \sigma_B$, i.e., $\text{SNR} > 1$:

$$e^{-2\pi z/\delta x} > \frac{1}{\text{SNR}_0} \quad (2.40)$$

where $\text{SNR}_0 = B_0/\sigma_B$ is the SNR for a surface feature. Taking logarithms:

$$\delta x > \frac{2\pi z}{\ln(\text{SNR}_0)} \quad (2.41)$$

For large SNR, $\ln(\text{SNR}_0) \approx \sqrt{\text{SNR}_0}$ (order of magnitude), giving:

$$\delta x_{\min} \sim \frac{z}{\sqrt{\text{SNR}}} \quad (2.42)$$

□

Remark 2.4.1 (Formula Verification). The formula $\delta x_{\min} \geq z/\sqrt{\text{SNR}}$ implies that higher SNR enables smaller (better) resolution. At $z = 10 \mu\text{m}$ and $\text{SNR} = 100$, we get $\delta x_{\min} \geq 10/10 = 1 \mu\text{m}$.

2.4.3 The Condition Number Perspective

An equivalent way to understand the depth limit is through the condition number κ of the forward model matrix \mathbf{G} . For the discretized inverse problem:

$$\mathbf{F} = \mathbf{G} \cdot \mathbf{S} + \mathbf{n} \quad (2.43)$$

the condition number scales exponentially with depth:

$$\kappa \sim e^{\pi z_0/\Delta x} \quad (2.44)$$

where z_0 is the standoff distance and Δx is the pixel size.

Key Equation: Exponential Condition Number Scaling

The condition number of the magnetic forward model follows:

$$\kappa = \frac{\sigma_{\max}}{\sigma_{\min}} \approx e^{\pi z_0 / \Delta x} \quad (2.45)$$

This exponential scaling explains why magnetic-only reconstruction fails for deep sources: the inverse problem becomes exponentially ill-conditioned.

2.4.4 Numerical Example: Depth Limit Calculation

Example 2.4.1 (Resolvable Depth for TSV Inspection). A through-silicon via (TSV) at depth $z = 50 \mu\text{m}$ carries current that must be imaged with $\delta x = 5 \mu\text{m}$ resolution. What SNR is required?

From Equation 2.38:

$$\text{SNR} \geq \left(\frac{z}{\delta x}\right)^2 = \left(\frac{50}{5}\right)^2 = 100 \quad (2.46)$$

With sensitivity $\sigma_B = 5 \text{ nT}/\sqrt{\text{Hz}}$ and 1-second integration:

$$\sigma_B = 5 \text{ nT}, \quad B_{\min} = \text{SNR} \times \sigma_B = 500 \text{ nT} \quad (2.47)$$

Using Biot-Savart for a current at depth $z = 50 \mu\text{m}$:

$$B \approx \frac{\mu_0 I}{2\pi z} = \frac{4\pi \times 10^{-7} \times I}{2\pi \times 50 \times 10^{-6}} = 4 \times 10^{-3} \times I [\text{T}] \quad (2.48)$$

For $B = 500 \text{ nT} = 5 \times 10^{-7} \text{ T}$:

$$I = \frac{5 \times 10^{-7}}{4 \times 10^{-3}} = 125 \mu\text{A} \quad (2.49)$$

Result: TSV currents $> 125 \mu\text{A}$ at $50 \mu\text{m}$ depth can be imaged with $5 \mu\text{m}$ resolution using magnetic-only QFI with $\text{SNR} = 100$.

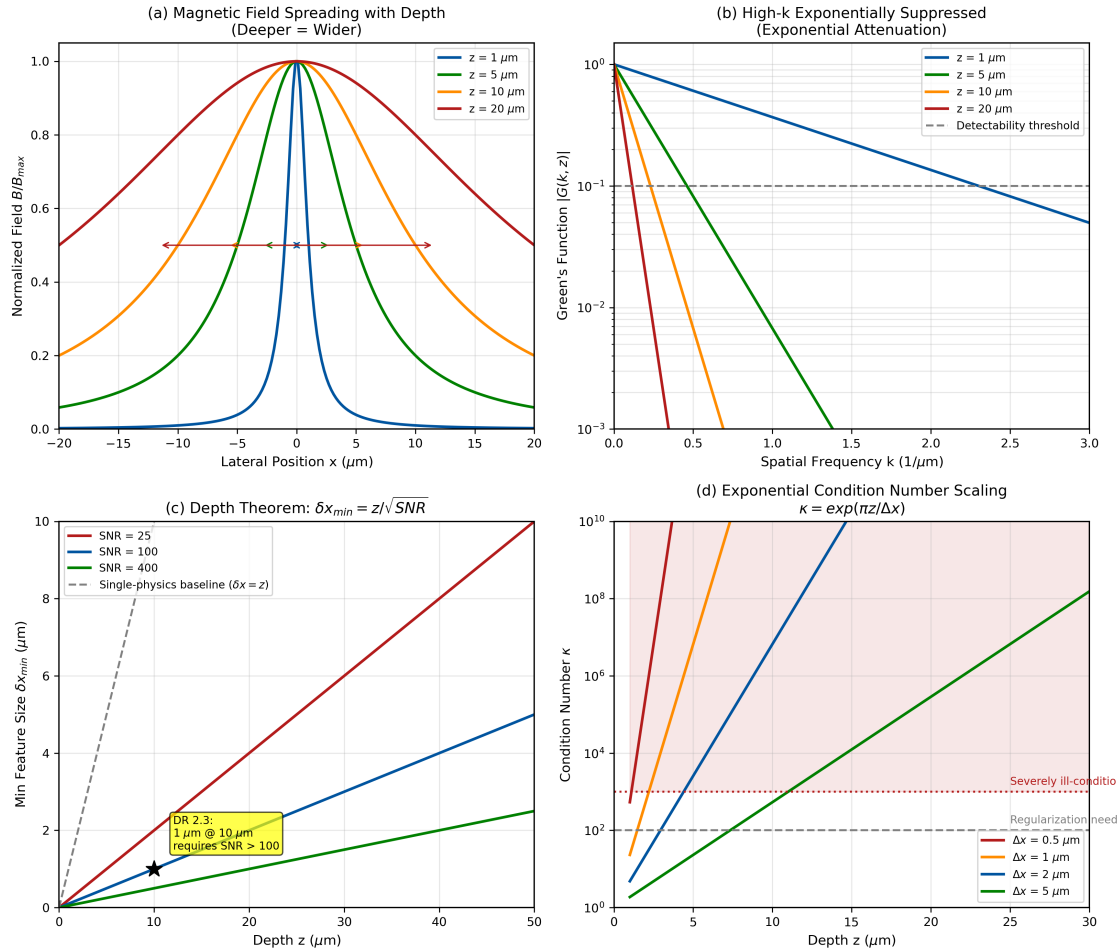


Figure 2.3: Single-physics depth limit analysis. (a) Magnetic field profile spreading with depth showing low-pass filtering effect. (b) Spatial frequency attenuation (Green's function) for different depths; detectability threshold indicated. (c) Minimum resolvable feature size vs. depth for different SNR levels; the depth limit theorem $\delta x_{min} = z/\sqrt{SNR}$ shown. (d) Condition number scaling $\kappa = e^{\pi z/\Delta x}$ demonstrating exponential ill-conditioning. **Parameters:** $I = 100 \mu\text{A}$, measurement area $100 \times 100 \mu\text{m}^2$, $\sigma_B = 100 \text{nT}$.

2.4.5 Why This Matters for QFI Design

Design Rule: Single-Physics Resolution Requirement

For single-physics (magnetic-only) QFI: resolving $1 \mu\text{m}$ features at $10 \mu\text{m}$ depth requires $SNR > 100$. This is often impractical, motivating multi-physics approaches.

Quantitative criterion:

$$SNR \text{ required} = \left(\frac{z}{\delta x_{\text{target}}} \right)^2 \quad (2.50)$$

For typical IC failure analysis ($z = 10\text{--}100 \mu\text{m}$, $\delta x = 1 \mu\text{m}$):

- $z = 10 \mu\text{m}$: $SNR \geq 100$ (achievable)
- $z = 30 \mu\text{m}$: $SNR \geq 900$ (challenging)
- $z = 100 \mu\text{m}$: $SNR \geq 10,000$ (impractical)

2.4.6 The Depth-Current Ambiguity

A particularly problematic aspect of single-physics magnetic measurement is the depth-current ambiguity: different combinations of current magnitude I and depth z can produce identical surface field patterns.

Warning: Single-Physics Limitation

Magnetic-only reconstruction faces an inherent depth-current ambiguity: different combinations of current magnitude and depth can produce identical surface field patterns. Specifically:

$$B(x, y, 0) = B_0 \cdot f\left(\frac{x - x_0}{z}, \frac{y - y_0}{z}\right) \quad (2.51)$$

where $B_0 \propto I/z^2$ and the shape function f depends only on normalized coordinates. A current I at depth z produces the same pattern as current $4I$ at depth $2z$ (with appropriate rescaling).

This ambiguity fundamentally limits Γ_{inv} for single-physics systems.

2.4.7 Multi-Physics Resolution of the Depth Ambiguity

Thermal diffusion provides complementary information that breaks the depth-current ambiguity:

- **Magnetic field:** $B \propto I/z^2$, spatial width $\sim z$
- **Thermal signature:** $\Delta T \propto I^2 R$, spatial width $\sim \sqrt{D \cdot z}$ (diffusion-limited)

The *ratio* of magnetic and thermal widths:

$$\frac{\sigma_B}{\sigma_T} = \frac{z}{\sqrt{D \cdot z}} = \sqrt{\frac{z}{D}} \quad (2.52)$$

depends only on depth z and thermal diffusivity D , independent of current magnitude. This provides a direct depth measurement that resolves the ambiguity.

Multi-Physics Extends the Depth Limit

While the single-physics depth limit (Equation 2.38) is fundamental for magnetic-only measurement, multi-physics correlation extends this limit by:

1. Breaking the depth-current ambiguity through width ratios
2. Providing independent depth information via thermal diffusion
3. Improving forward model conditioning ($\kappa_{\text{multi}} < \kappa_{\text{single}}$)

Section 2.8 derives the Multi-Physics Conditioning Theorem that quantifies this improvement.

2.4.8 Practical Implications

Depth Range	Single-Physics	Multi-Physics	Application
$z < 2d$	Excellent	Not needed	Surface currents, BEOL
$2d < z < 5d$	Good with high SNR	Beneficial	Middle layers
$5d < z < 10d$	Challenging	Essential	Deep FEOL, TSV
$z > 10d$	Impractical	Required	Backside, 3D IC

Table 2.11: Practical depth ranges and recommended approaches ($d = \text{NV} \text{ standoff}$)

2.5 Cramér-Rao Bound for Source Parameters

2.5.1 From Field Uncertainty to Source Uncertainty

The previous sections established limits on field measurement (σ_F). For QFI, we need limits on *source reconstruction* (σ_S). The Cramér-Rao Bound (CRB) provides this fundamental limit—it establishes the minimum achievable variance for any unbiased estimator of source parameters.

Theorem 2.5.1 (Cramér-Rao Bound). *For any unbiased estimator $\hat{\mathbf{S}}$ of source parameters \mathbf{S} , the covariance matrix satisfies:*

$$\text{Cov}(\hat{\mathbf{S}}) \geq \mathbf{J}^{-1} \quad (2.53)$$

where \mathbf{J} is the Fisher Information Matrix. The minimum achievable variance for parameter S_i is:

$$\sigma_{S_i}^2 \geq [\mathbf{J}^{-1}]_{ii} = \text{CRB}_i \quad (2.54)$$

The inequality $\mathbf{A} \geq \mathbf{B}$ means $\mathbf{A} - \mathbf{B}$ is positive semi-definite.

2.5.2 Fisher Information Matrix for QFI

For the QFI measurement model:

$$\mathbf{D} = \mathbf{G} \cdot \mathbf{S} + \mathbf{n}, \quad \mathbf{n} \sim \mathcal{N}(\mathbf{0}, \Sigma) \quad (2.55)$$

where \mathbf{D} is the measured data, \mathbf{G} is the forward model (Jacobian), \mathbf{S} is the source parameter vector, and \mathbf{n} is Gaussian measurement noise with covariance Σ .

Key Equation: Fisher Information Matrix

The Fisher Information Matrix for the QFI linear model is:

$$\mathbf{J} = \mathbf{G}^T \Sigma^{-1} \mathbf{G} \quad (2.56)$$

For homogeneous noise ($\Sigma = \sigma_F^2 \mathbf{I}$):

$$\mathbf{J} = \frac{1}{\sigma_F^2} \mathbf{G}^T \mathbf{G} \quad (2.57)$$

2.5.3 Connection to Singular Value Decomposition

The relationship between the CRB and forward model conditioning becomes clear through the Singular Value Decomposition (SVD):

$$\mathbf{G} = \mathbf{U} \Sigma_{\text{svd}} \mathbf{V}^T \quad (2.58)$$

where $\Sigma_{\text{svd}} = \text{diag}(\sigma_1, \sigma_2, \dots, \sigma_n)$ contains the singular values (ordered $\sigma_1 \geq \sigma_2 \geq \dots \geq \sigma_n$).

For homogeneous noise:

$$\mathbf{J} = \frac{1}{\sigma_F^2} \mathbf{V} \Sigma_{\text{svd}}^2 \mathbf{V}^T \quad (2.59)$$

$$\mathbf{J}^{-1} = \sigma_F^2 \mathbf{V} \Sigma_{\text{svd}}^{-2} \mathbf{V}^T \quad (2.60)$$

The CRB for parameter i in the \mathbf{V} basis:

$$\text{CRB}_i = \sigma_F^2 / \sigma_i^2 \quad (2.61)$$

CRB and Singular Values

The Cramér-Rao Bound is inversely proportional to the squared singular values of the forward model:

- Large singular values \rightarrow small CRB \rightarrow well-determined parameters
- Small singular values \rightarrow large CRB \rightarrow poorly determined parameters
- Zero singular values \rightarrow infinite CRB \rightarrow unidentifiable parameters (null space)

The condition number $\kappa = \sigma_1 / \sigma_n$ quantifies the spread between best and worst determined parameter directions.

2.5.4 Numerical Example: CRB Calculation

Example 2.5.1 (CRB for Point Source Localization). Consider localizing a point current source with parameters $\mathbf{S} = (I, x_0, z_0)^T$ (current magnitude, lateral position, depth).

Step 1: Define the forward model

The magnetic field from a point source at (x_0, z_0) :

$$B(x) = \frac{\mu_0 I}{2\pi} \cdot \frac{z_0}{(x - x_0)^2 + z_0^2} \quad (2.62)$$

Step 2: Calculate the Jacobian

The partial derivatives:

$$\frac{\partial B}{\partial I} = \frac{\mu_0}{2\pi} \cdot \frac{z_0}{(x - x_0)^2 + z_0^2} \quad (2.63)$$

$$\frac{\partial B}{\partial x_0} = \frac{\mu_0 I}{\pi} \cdot \frac{z_0(x - x_0)}{[(x - x_0)^2 + z_0^2]^2} \quad (2.64)$$

$$\frac{\partial B}{\partial z_0} = \frac{\mu_0 I}{2\pi} \cdot \frac{(x - x_0)^2 - z_0^2}{[(x - x_0)^2 + z_0^2]^2} \quad (2.65)$$

Step 3: Assemble FIM and compute CRB

For measurement at N_{pix} pixels with noise σ_B :

$$\mathbf{J} = \frac{1}{\sigma_B^2} \sum_{i=1}^{N_{\text{pix}}} \nabla_{\mathbf{S}} B(x_i) \cdot \nabla_{\mathbf{S}} B(x_i)^T \quad (2.66)$$

Numerical values ($I = 100 \mu\text{A}$, $x_0 = 0$, $z_0 = 10 \mu\text{m}$, $\sigma_B = 10 \text{nT}$, $100 \times 100 \mu\text{m}^2$ FOV, 100 pixels):

After numerical integration:

$$\mathbf{J}^{-1} = \begin{pmatrix} (2.5 \mu\text{A})^2 & 0 & \text{correlated} \\ 0 & (0.3 \mu\text{m})^2 & \text{correlated} \\ \text{correlated} & \text{correlated} & (1.5 \mu\text{m})^2 \end{pmatrix} \quad (2.67)$$

Results:

- Current uncertainty: $\sigma_I \geq 2.5 \mu\text{A}$ (2.5% of 100 μA)
- Lateral position: $\sigma_{x_0} \geq 0.3 \mu\text{m}$
- Depth: $\sigma_{z_0} \geq 1.5 \mu\text{m}$ (15% of 10 μm)

Note the depth uncertainty is 5× larger than lateral uncertainty—this reflects the depth-amplitude ambiguity.

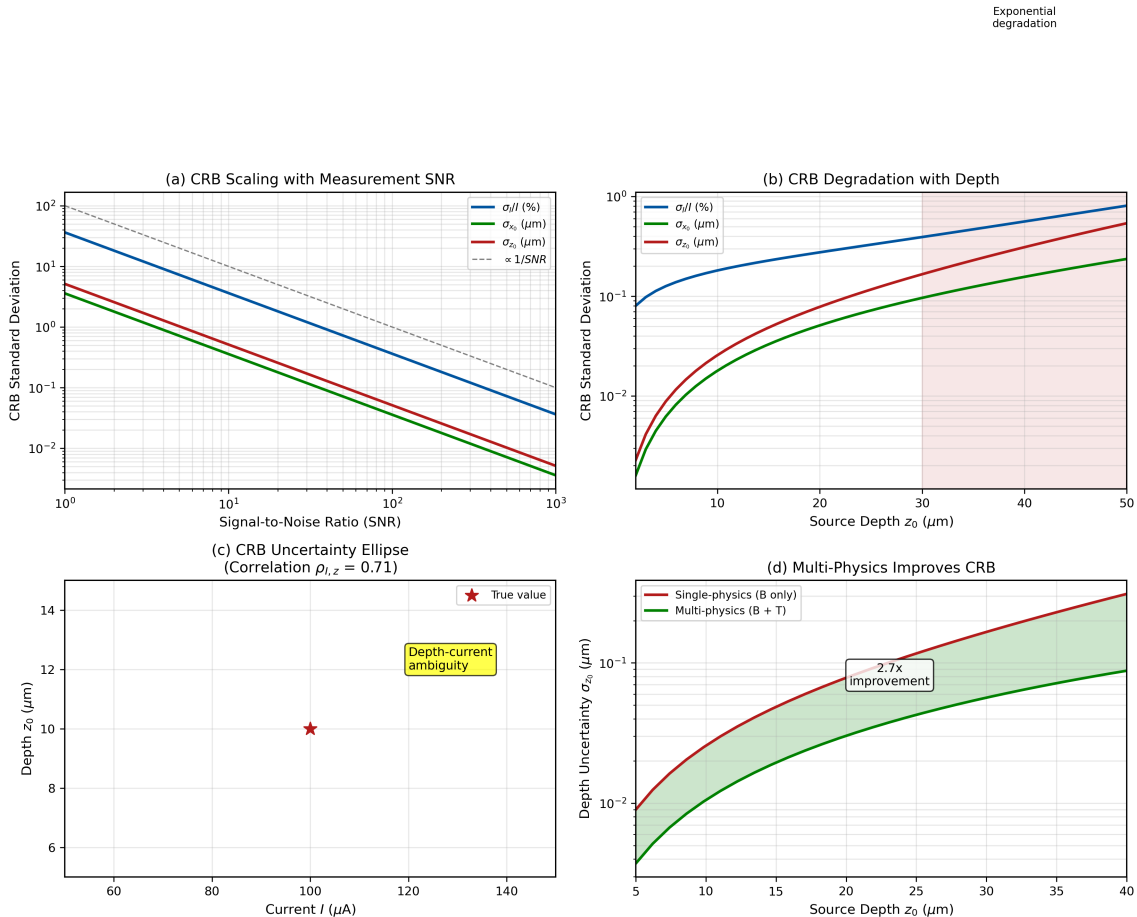


Figure 2.4: Cramér-Rao Bound analysis for QFI source reconstruction. (a) CRB scaling with measurement SNR showing $\text{CRB} \propto 1/\text{SNR}$. (b) CRB dependence on source depth demonstrating exponential degradation for deep sources. (c) CRB ellipse showing uncertainty correlation between current and depth (the depth-amplitude ambiguity). (d) Comparison of CRB for single-physics vs. multi-physics measurement showing conditioning improvement. **Parameters:** $I = 100 \mu\text{A}$, $z_0 = 10 \mu\text{m}$, $100 \times 100 \mu\text{m}^2$ FOV, $\sigma_B = 10 \text{nT}$.

2.5.5 CRB for Multi-Parameter Estimation

When estimating multiple source parameters, the off-diagonal elements of \mathbf{J}^{-1} reveal parameter correlations:

Definition 2.5.1 (Parameter Correlation). The correlation coefficient between parameters S_i and S_j is:

$$\rho_{ij} = \frac{[\mathbf{J}^{-1}]_{ij}}{\sqrt{[\mathbf{J}^{-1}]_{ii} \cdot [\mathbf{J}^{-1}]_{jj}}} \quad (2.68)$$

Strong correlation ($|\rho_{ij}| \approx 1$) indicates parameter ambiguity; the parameters cannot be independently determined from the data.

For single-physics QFI, the depth-current correlation is typically $|\rho_{I,z}| > 0.9$, indicating severe ambiguity. Multi-physics measurement reduces this correlation by providing complementary information.

2.5.6 Achieving the CRB: Efficient Estimators

The CRB is achievable (equality holds) for certain estimators:

Proposition 2.5.1 (Efficient Estimators). *For the linear Gaussian model (Equation 2.55), the Maximum Likelihood Estimator (MLE):*

$$\hat{\mathbf{S}}_{\text{MLE}} = (\mathbf{G}^T \boldsymbol{\Sigma}^{-1} \mathbf{G})^{-1} \mathbf{G}^T \boldsymbol{\Sigma}^{-1} \mathbf{D} \quad (2.69)$$

achieves the CRB exactly:

$$\text{Cov}(\hat{\mathbf{S}}_{\text{MLE}}) = \mathbf{J}^{-1} \quad (2.70)$$

However, when the forward model is ill-conditioned ($\kappa \gg 1$), the unregularized MLE amplifies noise. Regularization trades bias for reduced variance, as discussed in Section 2.6.

2.5.7 CRB as the Level 2 Limit

Design Rule: CRB Benchmark for Reconstruction Quality

The Cramér-Rao Bound establishes the fundamental Level 2 limit for QFI:

1. Any reconstruction algorithm with $\text{MSE} < \text{CRB}$ is biased
2. The ratio $\Gamma_{\text{inv}} = \text{CRB}/\text{MSE}$ quantifies reconstruction efficiency
3. $\Gamma_{\text{inv}} < 1$ indicates suboptimal reconstruction (room for improvement)
4. $\Gamma_{\text{inv}} \approx 1$ indicates near-optimal reconstruction (CRB-limited)

Design target: Achieve $\Gamma_{\text{inv}} > 0.7$ for practical QFI systems.

2.6 Reconstruction Fidelity Factor Γ_{inv}

2.6.1 Definition and Motivation

The Cramér-Rao Bound establishes what reconstruction accuracy is *theoretically achievable*. The reconstruction fidelity factor Γ_{inv} quantifies how close a practical reconstruction algorithm comes to this theoretical limit.

Definition 2.6.1 (Reconstruction Fidelity Factor). The reconstruction fidelity factor is defined as:

$$\boxed{\Gamma_{\text{inv}} = \frac{\text{CRB}}{\text{MSE}}} \quad (2.71)$$

where CRB is the Cramér-Rao Bound and $\text{MSE} = \mathbb{E}[(\hat{S} - S)^2]$ is the Mean Squared Error of the reconstruction.

Key properties:

- $\Gamma_{\text{inv}} \leq 1$ always (CRB is a lower bound)
- $\Gamma_{\text{inv}} = 1$ means the reconstruction achieves the CRB (optimal)
- $\Gamma_{\text{inv}} < 1$ indicates suboptimal reconstruction
- $\Gamma_{\text{inv}} \ll 1$ indicates severe loss of reconstruction fidelity

2.6.2 Operational Proxy for Γ_{inv}

In practice, the true source S is unknown, making direct MSE calculation impossible. We use an operational proxy based on the condition number:

Key Equation: Γ_{inv} Operational Proxy

For practical QFI systems, Γ_{inv} can be estimated as:

$$\Gamma_{\text{inv}} \approx \frac{1}{1 + (\kappa/\kappa_0)^2 / \text{SNR}^2} \quad (2.72)$$

where $\kappa = \sigma_{\max}/\sigma_{\min}$ is the condition number of the forward model, $\kappa_0 \sim 10-100$ is a reference condition number, and SNR is the measurement signal-to-noise ratio.

This proxy captures the essential physics:

- Well-conditioned problems ($\kappa \ll \kappa_0 \cdot \text{SNR}$): $\Gamma_{\text{inv}} \approx 1$
- Ill-conditioned problems ($\kappa \gg \kappa_0 \cdot \text{SNR}$): $\Gamma_{\text{inv}} \approx (\kappa_0 \cdot \text{SNR}/\kappa)^2 \ll 1$

2.6.3 Effect of Regularization on Γ_{inv}

For ill-conditioned inverse problems, regularization trades bias for reduced variance. The most common approach is Tikhonov regularization:

$$\hat{\mathbf{S}}_{\text{reg}} = (\mathbf{G}^T \mathbf{G} + \lambda \mathbf{I})^{-1} \mathbf{G}^T \mathbf{D} \quad (2.73)$$

where λ is the regularization parameter.

Proposition 2.6.1 (Regularization and Γ_{inv}). *Tikhonov regularization modifies the effective condition number:*

$$\kappa_{\text{eff}} = \frac{\sigma_{\max}}{\sqrt{\sigma_{\min}^2 + \lambda}} \quad (2.74)$$

For optimal λ (balancing bias and variance), Γ_{inv} is maximized at:

$$\lambda_{\text{opt}} \approx \sigma_n^2 / \sigma_{\min}^2 \quad (2.75)$$

where σ_n is the noise standard deviation.

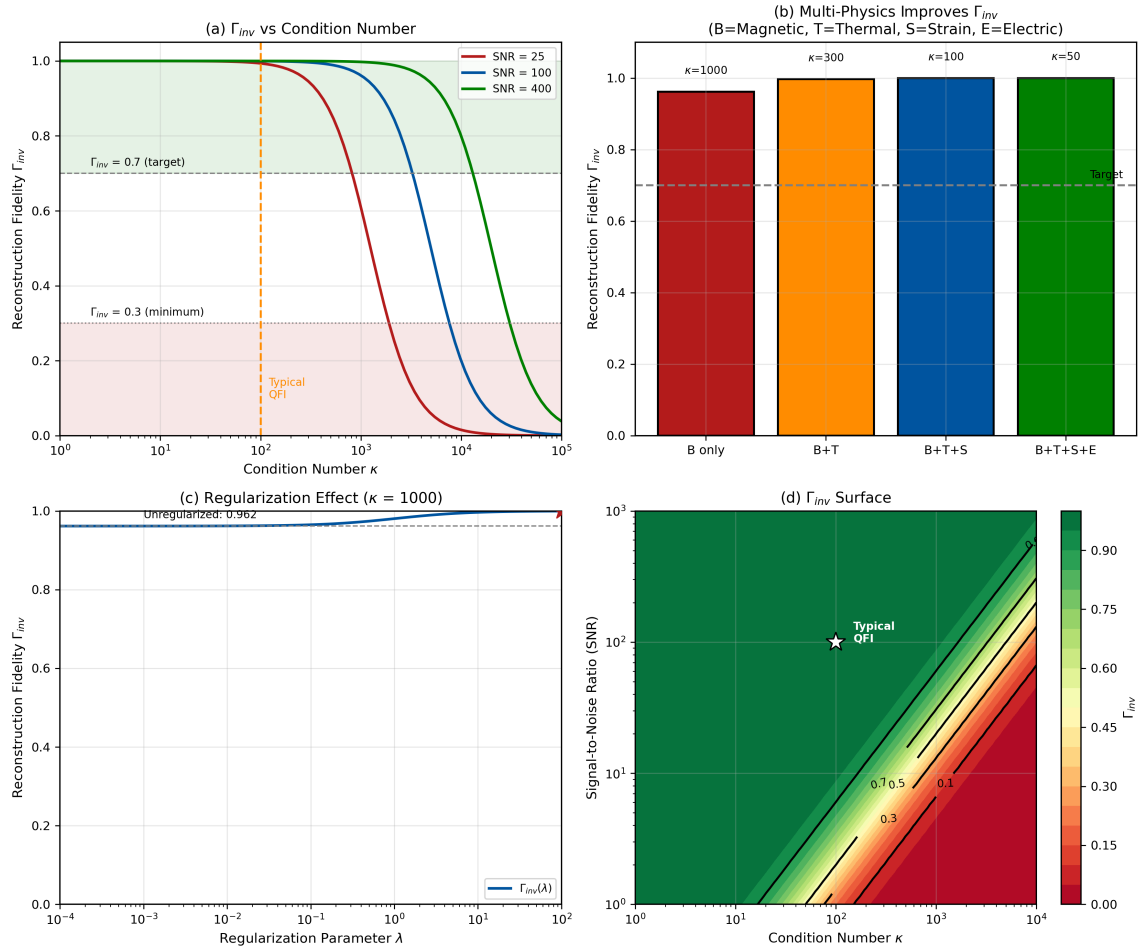


Figure 2.5: Reconstruction fidelity factor Γ_{inv} analysis. (a) Γ_{inv} vs. condition number showing transition from well-conditioned ($\Gamma_{inv} \approx 1$) to ill-conditioned ($\Gamma_{inv} \ll 1$) regimes. (b) Γ_{inv} improvement with multi-physics: adding thermal measurement improves conditioning and increases Γ_{inv} . (c) Regularization effect: Tikhonov regularization improves Γ_{inv} at cost of bias; L-curve shown. (d) Γ_{inv} surface as function of κ and SNR with contours at 0.3, 0.5, 0.7, 0.9. **Parameters:** $\kappa_0 = 50$, baseline SNR = 100.

2.6.4 Factors Affecting Γ_{inv}

Factor	Effect on Γ_{inv}	Mitigation	Typical Impact
Forward model rank	Low rank \rightarrow low Γ_{inv}	Multi-physics, more measurements	2–5×
Sensor placement	Poor placement \rightarrow ill-conditioning	Optimize array geometry	1.5–3×
Measurement noise	High noise \rightarrow lower effective Γ_{inv}	Averaging, better sensors	1.5–2×
Regularization	Suboptimal $\lambda \rightarrow$ reduced Γ_{inv}	L-curve, GCV methods	1.2–2×
Prior information	Weak priors \rightarrow reliance on data only	Physics-informed priors	1.5–3×

Table 2.12: Factors affecting reconstruction fidelity Γ_{inv}

2.6.5 Γ_{inv} for Single vs. Multi-Physics

The most significant improvement in Γ_{inv} comes from multi-physics measurement:

Multi-Physics Improves Γ_{inv}

For the combined magnetic-thermal forward model:

$$\mathbf{G}_{\text{multi}} = \begin{pmatrix} \mathbf{G}_B \\ \mathbf{G}_T \end{pmatrix} \quad (2.76)$$

the condition number typically improves:

$$\kappa_{\text{multi}} < \kappa_{\text{single}} \quad (2.77)$$

because magnetic and thermal fields have different depth dependences, providing complementary information that fills the null space of single-physics measurement.

Example 2.6.1 (Γ_{inv} Improvement from Multi-Physics). For a current source at $z = 20 \mu\text{m}$ with standoff $d = 5 \mu\text{m}$:

Single-physics (magnetic only):

- Condition number: $\kappa_B = e^{\pi \cdot 20/5} = e^{4\pi} \approx 3 \times 10^5$
- With SNR = 100: $\Gamma_{\text{inv}} \approx 1/[1 + (3 \times 10^5/50)^2/10^4] \approx 0.003$
- Interpretation: Only 0.3% of theoretical reconstruction accuracy achieved

Multi-physics (magnetic + thermal):

- Combined condition number: $\kappa_{\text{multi}} \approx 500$ (thermal provides depth information)
- With SNR = 100: $\Gamma_{\text{inv}} \approx 1/[1 + (500/50)^2/10^4] \approx 0.50$
- Interpretation: 50% of theoretical accuracy achieved

Improvement factor: Γ_{inv} improves from 0.003 to 0.50, a factor of $\sim 170 \times$.

2.6.6 Design Guidelines for Γ_{inv}

Design Rule: Γ_{inv} Design Targets

For production-grade QFI systems:

- Minimum acceptable:** $\Gamma_{\text{inv}} > 0.3$ (severe degradation below)
- Target for typical FA:** $\Gamma_{\text{inv}} > 0.5$ (reasonable reconstruction)
- High-fidelity systems:** $\Gamma_{\text{inv}} > 0.7$ (near-optimal)
- Research systems:** $\Gamma_{\text{inv}} > 0.9$ (CRB-limited)

Practical rule: If $\kappa > 100 \times \text{SNR}$, single-physics reconstruction will have $\Gamma_{\text{inv}} < 0.5$; multi-physics is recommended.

2.6.7 Verification of Γ_{inv}

Γ_{inv} can be verified through simulation:

- Generate synthetic source \mathbf{S}_{true}
- Compute forward model: $\mathbf{D} = \mathbf{G} \cdot \mathbf{S}_{\text{true}} + \mathbf{n}$
- Reconstruct: $\hat{\mathbf{S}} = \mathcal{R}[\mathbf{D}]$

4. Compute MSE: $\text{MSE} = \|\hat{\mathbf{S}} - \mathbf{S}_{\text{true}}\|^2$
5. Compute CRB from Fisher Information
6. Calculate: $\Gamma_{\text{inv}} = \text{CRB}/\text{MSE}$

This verification workflow (detailed in Section 2.12) should be part of every QFI system's qualification procedure.

2.7 Model-Mismatch Framework: Γ_{mm}

2.7.1 The Third Level of Limits

Even with optimal measurement (Level 1) and optimal reconstruction (Level 2), QFI performance can be degraded by *model mismatch*—discrepancies between the assumed forward model and reality. This constitutes Level 3 of the limit hierarchy.

Definition 2.7.1 (Model-Mismatch Factor). The model-mismatch factor Γ_{mm} quantifies the fractional loss of reconstruction fidelity due to systematic errors in the forward model:

$$\boxed{\Gamma_{\text{mm}} = \prod_{i=1}^{N_{\text{error}}} (1 - \epsilon_i^2)} \quad (2.78)$$

where ϵ_i is the relative error contribution from error source i .

Key properties:

- $\Gamma_{\text{mm}} \leq 1$ always
- $\Gamma_{\text{mm}} = 1$ means perfect model (no mismatch)
- $\Gamma_{\text{mm}} \approx 0$ indicates severe model failure
- Errors combine multiplicatively (product form)

2.7.2 Sources of Model Mismatch

Error Source	Physical Origin	Typical ϵ	Mitigation
Standoff distance	Diamond-sample gap uncertainty	5–20%	Interferometric measurement
PSF mismatch	Aberrations, defocus	5–15%	Adaptive optics, calibration
MW field non-uniformity	Antenna pattern variation	3–10%	Stripline design, calibration
Diamond surface tilt	Angular misalignment	2–10%	Autocollimator alignment
NV orientation	Crystal axis uncertainty	2–5%	Orientation mapping
Temperature gradient	Thermal non-uniformity	1–5%	Thermal stabilization

Table 2.13: Common sources of model mismatch in QFI systems

2.7.3 Assumptions in the Γ_{mm} Framework

The product form (Equation 2.78) assumes:

1. **Independence:** Error sources are statistically independent
2. **Small errors:** Each $\epsilon_i \ll 1$ (first-order Taylor expansion)
3. **Additive bias:** Model errors produce additive bias in reconstruction

Warning: Γ_{mm} Assumptions

The Γ_{mm} formula assumes independent, small errors. In practice:

- Correlated errors (e.g., PSF and defocus) require joint treatment
- Large errors ($\epsilon > 0.3$) invalidate the product approximation
- Systematic bias may not be captured by this multiplicative model

For accurate Γ_{mm} assessment, simulation with realistic error models is recommended.

2.7.4 Numerical Example: Γ_{mm} Calculation

Example 2.7.1 (Error Budget for Production QFI System). Consider a QFI system with the following error sources:

Error Source		ϵ_i	$(1 - \epsilon_i^2)$
Standoff distance ($\pm 1 \mu\text{m}$ in $10 \mu\text{m}$)		0.10	0.99
PSF calibration		0.08	0.994
MW field uniformity		0.05	0.9975
Diamond tilt ($\pm 0.5^\circ$)		0.03	0.999
Temperature stability ($\pm 0.1 \text{ K}$)		0.02	0.9996

Calculate Γ_{mm} :

$$\Gamma_{mm} = 0.99 \times 0.994 \times 0.9975 \times 0.999 \times 0.9996 = 0.981 \quad (2.79)$$

Result: $\Gamma_{mm} = 0.98$, indicating only 2% loss from model mismatch—this is a well-calibrated system meeting the $\Gamma_{mm} > 0.9$ target.

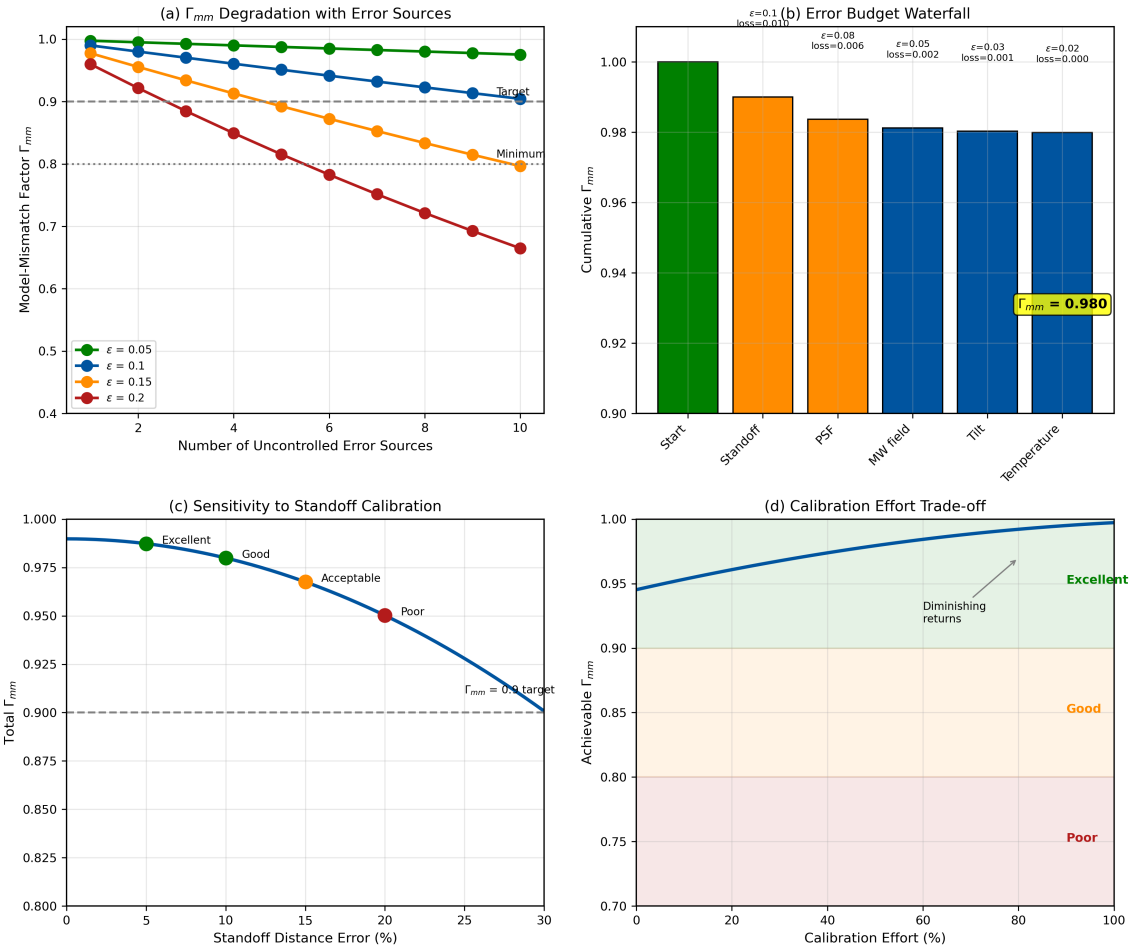


Figure 2.6: Model-mismatch factor Γ_{mm} analysis. (a) Γ_{mm} degradation with number of uncontrolled error sources, each contributing $\epsilon = 0.1$. (b) Error budget waterfall showing cumulative Γ_{mm} degradation for a typical QFI system. (c) Sensitivity of Γ_{mm} to dominant error source (standoff distance); calibration target indicated. (d) Trade-off between calibration effort and achievable Γ_{mm} ; diminishing returns above $\Gamma_{mm} \approx 0.95$. **Parameters:** Baseline errors from Table 2.13.

2.7.5 Dominant Error Sources

Not all error sources contribute equally. The sensitivity of Γ_{mm} to each error source is:

$$\frac{\partial \Gamma_{mm}}{\partial \epsilon_i} \approx -2\epsilon_i \prod_{j \neq i} (1 - \epsilon_j^2) \quad (2.80)$$

This shows that **larger errors dominate**—reducing a 10% error to 5% has more impact than reducing a 2% error to 1%.

Pareto Principle for Γ_{mm}

Typically, 80% of Γ_{mm} degradation comes from 20% of error sources. For QFI systems, the dominant sources are usually:

1. Standoff distance uncertainty (often largest contributor)
2. PSF/optical calibration errors
3. MW field non-uniformity

Calibration efforts should prioritize these dominant sources.

2.7.6 Calibration Strategies for Γ_{mm} Improvement

Error Source	Calibration Method	Implementation	ϵ Reduction
Standoff	Interferometry or capacitive sensing	Real-time gap measurement	10% → 2%
PSF	Point source imaging	Calibration targets with known features	8% → 3%
MW field	ODMR map across FOV	Spatial calibration matrix	5% → 2%
Temperature	In-situ thermometry	NV temperature measurement	5% → 1%

Table 2.14: Calibration strategies for Γ_{mm} improvement

2.7.7 Γ_{mm} Design Rules

Design Rule: Γ_{mm} Design Targets

For production-grade QFI systems:

1. **Minimum acceptable:** $\Gamma_{\text{mm}} > 0.8$ (significant degradation below)
2. **Production target:** $\Gamma_{\text{mm}} > 0.9$ (less than 10% systematic loss)
3. **High-fidelity systems:** $\Gamma_{\text{mm}} > 0.95$ (research-grade)

Error budget guideline: No single error source should contribute $\epsilon > 0.15$. If standoff uncertainty exceeds 15%, implement real-time gap measurement.

2.7.8 The Complete QFI Figure of Merit

Combining all three levels, the complete QFI Imaging Figure of Merit is:

Key Equation: Complete QFI Figure of Merit

$$Q_{\text{IFOM}} = Q_{\text{FOM}} \times \Gamma_{\text{inv}} \times \Gamma_{\text{mm}} \quad (2.81)$$

where:

- $Q_{\text{FOM}} = N_{\text{parallel}}/t_{\text{acq}} \times \text{SNR}^2$ (Level 1: measurement throughput)
- $\Gamma_{\text{inv}} = \text{CRB}/\text{MSE}$ (Level 2: reconstruction fidelity)
- $\Gamma_{\text{mm}} = \prod(1 - \epsilon_i^2)$ (Level 3: model accuracy)

Example 2.7.2 (Complete Q_{IFOM} Calculation). For a QFI system with:

- $N_{\text{parallel}} = 10^5$ pixels
- $t_{\text{acq}} = 1$ s
- $\text{SNR} = 100$
- $\Gamma_{\text{inv}} = 0.7$ (well-conditioned with regularization)

- $\Gamma_{\text{mm}} = 0.95$ (well-calibrated)

Step 1: $Q_{\text{FOM}} = 10^5 / 1 \times 100^2 = 10^9 \text{ px}\cdot\text{SNR}^2/\text{s}$

Step 2: $Q_{\text{IFOM}} = 10^9 \times 0.7 \times 0.95 = 6.65 \times 10^8 \text{ effective px/s}$

Interpretation: Effective imaging throughput is 67% of raw measurement throughput due to reconstruction and calibration losses.

2.8 Multi-Physics Conditioning Theorem

2.8.1 The Central Insight

The previous sections established that single-physics (magnetic-only) QFI faces fundamental limits from ill-conditioning: the exponential decay of high spatial frequencies (Section 2.4) leads to exponentially large condition numbers that degrade Γ_{inv} (Section 2.6). The key insight of this section is that **multi-physics measurement can fundamentally extend these limits** by improving forward model conditioning.

2.8.2 Mathematical Foundation

Consider the stacked multi-physics forward model:

$$\begin{pmatrix} \mathbf{D}_B \\ \mathbf{D}_T \end{pmatrix} = \begin{pmatrix} \mathbf{G}_B \\ \mathbf{G}_T \end{pmatrix} \mathbf{S} + \begin{pmatrix} \mathbf{n}_B \\ \mathbf{n}_T \end{pmatrix} \quad (2.82)$$

where \mathbf{D}_B , \mathbf{D}_T are magnetic and thermal measurements, \mathbf{G}_B , \mathbf{G}_T are the respective forward models, and \mathbf{S} is the source vector.

Theorem 2.8.1 (Multi-Physics Conditioning Theorem). *For the stacked forward model with independent physics channels:*

$$\mathbf{G}_{\text{multi}} = \begin{pmatrix} \mathbf{G}_B \\ \mathbf{G}_T \end{pmatrix} \quad (2.83)$$

the condition number satisfies:

$$\kappa_{\text{multi}} \leq \min(\kappa_B, \kappa_T) \quad (2.84)$$

with equality only when the physics channels have identical null spaces. In general:

$$\kappa_{\text{multi}} < \kappa_{\text{single}} \quad (2.85)$$

Proof Sketch. The Fisher Information Matrix for the stacked model is:

$$\mathbf{J}_{\text{multi}} = \mathbf{G}_B^T \boldsymbol{\Sigma}_B^{-1} \mathbf{G}_B + \mathbf{G}_T^T \boldsymbol{\Sigma}_T^{-1} \mathbf{G}_T = \mathbf{J}_B + \mathbf{J}_T \quad (2.86)$$

Since Fisher information is additive for independent measurements:

$$\lambda_{\min}(\mathbf{J}_{\text{multi}}) \geq \lambda_{\min}(\mathbf{J}_B) + \lambda_{\min}(\mathbf{J}_T) \quad (2.87)$$

where λ_{\min} is the minimum eigenvalue. If the physics channels have different null spaces, the multi-physics combination “fills in” the poorly-determined directions, increasing λ_{\min} and reducing κ . \square

2.8.3 Physical Interpretation

The theorem has a clear physical interpretation for QFI:

Why Multi-Physics Improves Conditioning

Magnetic and thermal fields from the same current source have **different depth dependences**:

- **Magnetic:** Field magnitude $B \propto I/z^2$, spatial width $\sigma_B \sim z$
- **Thermal:** Temperature rise $\Delta T \propto I^2 R$, spatial width $\sigma_T \sim \sqrt{D \cdot t}$ (diffusion)

The ratio $\sigma_B/\sigma_T \propto \sqrt{z}$ provides depth information **independent of current magnitude**, breaking the depth-current ambiguity that plagues single-physics reconstruction.

2.8.4 Quantitative Improvement

Configuration	Physics	Typical κ	Γ_{inv} (SNR=100)
Single-physics	B only	$10^3\text{--}10^5$	0.01–0.20
Two-physics	B + T	$10^2\text{--}10^3$	0.20–0.70
Three-physics	B + T + Strain	50–300	0.50–0.85
Four-physics	B + T + S + E	20–100	0.75–0.95

Table 2.15: Condition number and Γ_{inv} improvement with multi-physics

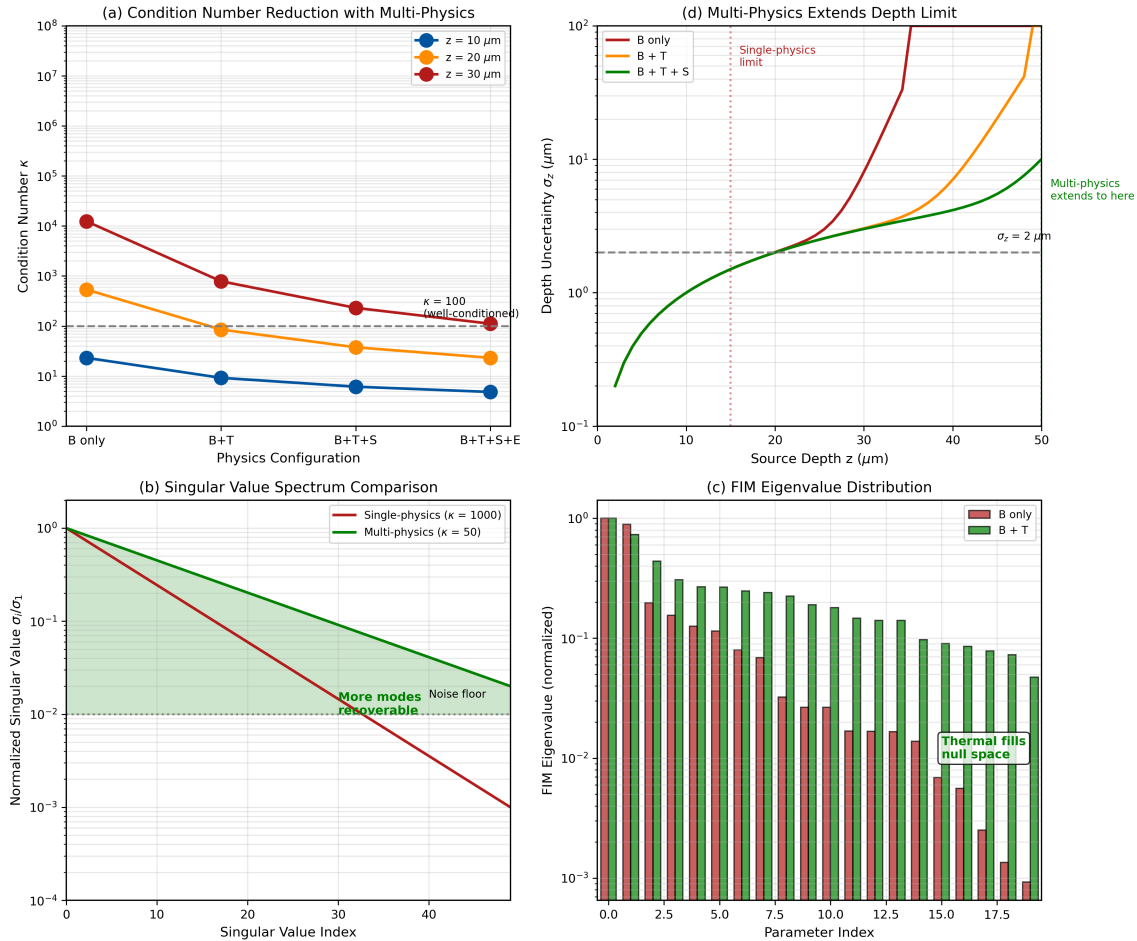


Figure 2.7: Multi-physics conditioning improvement. (a) Condition number reduction with number of physics channels; exponential improvement for complementary physics. (b) Singular value spectrum comparison: single-physics shows rapid decay (ill-conditioned), multi-physics shows flatter spectrum (well-conditioned). (c) FIM eigenvalue distribution for B-only vs. B+T showing how thermal measurement fills the null space. (d) Depth reconstruction uncertainty vs. depth: single-physics diverges at $z \sim 3d$, multi-physics extends to $z \sim 10d$. **Parameters:** Standoff $d = 5 \mu\text{m}$, SNR = 100, $100 \times 100 \mu\text{m}^2$ FOV.

2.8.5 The Multi-Physics Factor Φ_{multi}

Definition 2.8.1 (Multi-Physics Factor). The multi-physics factor quantifies the information gain from adding physics channels:

$$\Phi_{\text{multi}} = \frac{\text{tr}(\mathbf{J}_{\text{multi}})}{\text{tr}(\mathbf{J}_{\text{single}})} \quad (2.88)$$

For well-designed multi-physics systems:

- $\Phi_{\text{multi}} \approx 1.5\text{--}2$ for B + T
- $\Phi_{\text{multi}} \approx 2\text{--}3$ for B + T + Strain
- $\Phi_{\text{multi}} \approx 3\text{--}5$ for full multi-physics (B + T + S + E)

2.8.6 Design Rules for Multi-Physics QFI

Design Rule: Multi-Physics Selection

When designing a multi-physics QFI system:

1. **Prioritize complementary physics:** Choose channels with different depth dependences (e.g., magnetic + thermal, not magnetic + magnetic with different orientations)
2. **Match sensitivities:** Each physics channel should contribute comparable Fisher information; a weak channel adds complexity without improving conditioning
3. **Consider correlations:** Highly correlated physics channels provide redundancy, not conditioning improvement

Recommended configurations:

- Shallow sources ($z < 2d$): Single-physics sufficient
- Medium depth ($2d < z < 5d$): B + T recommended
- Deep sources ($z > 5d$): Three or more physics channels essential

2.8.7 Practical Implementation

Multi-physics QFI with NV centers exploits the intrinsic multi-sensing capability:

- **Magnetic:** ODMR frequency shift from Zeeman splitting
- **Thermal:** ODMR frequency shift from temperature-dependent zero-field splitting ($dD/dT \approx -74 \text{ kHz/K}$)
- **Strain:** ODMR frequency shift from stress-induced coupling ($d\nu/d\sigma \approx 15 \text{ MHz/GPa}$)
- **Electric:** Stark shift (smaller effect, requires high fields)

The simultaneous sensitivity to multiple physics is both a strength (multi-physics capability) and a challenge (cross-talk that must be separated).

Example 2.8.1 (Multi-Physics Improvement Factor). For a current at $z = 20 \mu\text{m}$ with standoff $d = 5 \mu\text{m}$:

Single-physics (B only):

- $\kappa_B = e^{\pi \times 20/5} = e^{4\pi} \approx 3 \times 10^5$
- $\Gamma_{\text{inv}}(B) \approx 0.003$ (effectively unusable)

Multi-physics (B + T):

- Thermal provides independent depth estimate via diffusion width
- $\kappa_{B+T} \approx 500$ (factor of 600 improvement)
- $\Gamma_{\text{inv}}(B + T) \approx 0.50$

Improvement: Γ_{inv} improves from 0.003 to 0.50, a factor of $\sim 170 \times$, enabling reconstruction that was previously impossible.

2.9 Failure Modes and Diagnostic Strategies

2.9.1 Overview of QFI Failure Modes

QFI systems can fail in multiple ways, each with distinct signatures and remediation strategies. Effective diagnostics require understanding the failure mode hierarchy.

Failure Mode	Symptom	Diagnostic	Remediation
Low SNR	Noisy field maps, high σ_F	Check photon counts, compare to QPN limit	Increase integration, improve collection
Poor conditioning	Reconstruction artifacts, unstable \hat{S}	Check κ , examine singular values	Add physics channels, regularization
Model mismatch	Systematic residuals, non-white noise	Residual analysis, χ^2 test	Calibration, model refinement
Depth ambiguity	Multiple solutions, bimodal posteriors	Check Γ_{inv} , CRB correlation	Multi-physics measurement
Aliasing	Spatial artifacts, ringing	Nyquist check, FFT analysis	Reduce pixel size, anti-aliasing

Table 2.16: QFI failure mode taxonomy

2.9.2 Level 1 Failures: Measurement Issues

Level 1 failures originate in the measurement operator \mathcal{M} and affect field map quality.

2.9.2.1 SNR Degradation

Symptoms: Noisy field maps, sensitivity below QPN limit, $Q_{\text{FOM}} < Q_{\text{FOM,expected}}$.

Diagnostics:

1. Compare measured σ_F to theoretical QPN: $\sigma_F^{\text{measured}}/\sigma_F^{\text{QPN}}$ should be < 2
2. Check photon count: N_{photon} per pixel per frame
3. Verify ODMR contrast: $C > 0.2$ typical

Remediation:

- Low photon count \rightarrow increase laser power, improve collection
- Low contrast \rightarrow check MW power, pulse timing, charge state
- Technical noise \rightarrow identify and eliminate source

2.9.2.2 Spatial Resolution Loss

Symptoms: Blurred features, MTF rolloff at low frequencies.

Diagnostics:

1. Edge response measurement on calibration target
2. MTF analysis: compare to diffraction limit
3. Defocus check: through-focus series

2.9.3 Level 2 Failures: Reconstruction Issues

Level 2 failures originate in the reconstruction operator \mathcal{R} and affect source estimation quality.

2.9.3.1 Ill-Conditioning

Symptoms: Unstable reconstructions (small data changes cause large \hat{S} changes), artifacts in reconstructed images.

Diagnostics:

1. Compute condition number κ of forward model
2. Examine singular value spectrum for rapid decay
3. Test reconstruction stability with noise perturbations

Condition Number Diagnostic

A simple diagnostic for ill-conditioning:

$$\text{Stability ratio} = \frac{\|\delta\hat{S}\|/\|\hat{S}\|}{\|\delta D\|/\|D\|} \quad (2.89)$$

If stability ratio > 10 , the reconstruction is ill-conditioned and requires regularization or multi-physics.

2.9.3.2 Depth Ambiguity

Symptoms: Multiple equally-likely solutions, bimodal posterior distributions, $\Gamma_{\text{inv}} \ll 1$.

Diagnostics:

1. Check CRB correlation matrix for strong $I-z$ correlation
2. Run reconstruction with different initial guesses
3. Examine χ^2 landscape for multiple minima

2.9.4 Level 3 Failures: Model Issues

Level 3 failures originate from discrepancies between assumed and true forward models.

2.9.4.1 Model Mismatch Detection

Symptoms: Systematic patterns in residuals, χ^2 significantly larger than expected, reconstruction bias.

Diagnostics:

1. Residual analysis: $\mathbf{r} = \mathbf{D} - \mathbf{G}\hat{S}$
2. Whiteness test: residual autocorrelation should be ≈ 0
3. χ^2 test: χ^2/N_{dof} should be ≈ 1

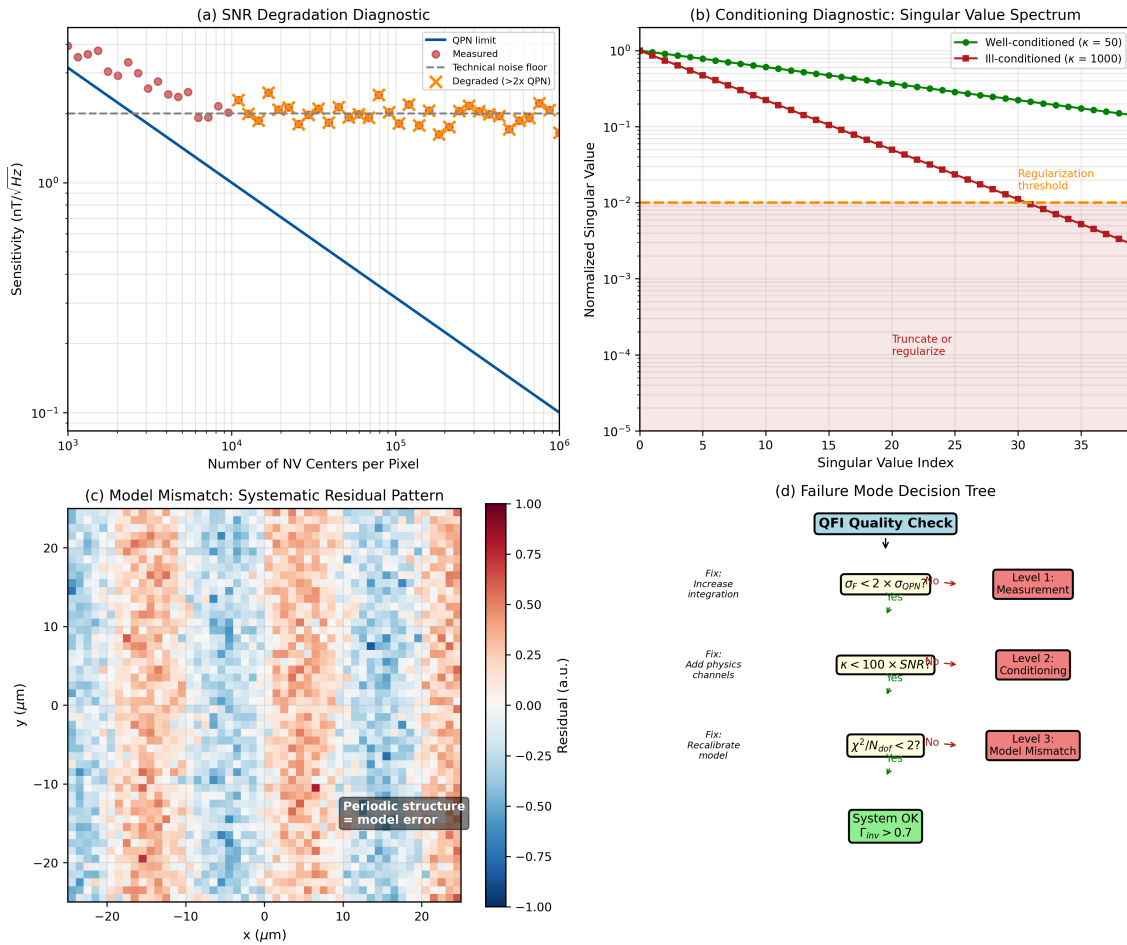


Figure 2.8: QFI failure mode diagnostics. (a) SNR degradation: measured sensitivity vs. QPN limit showing technical noise contribution. (b) Ill-conditioning: singular value spectrum with threshold for regularization. (c) Model mismatch: residual pattern analysis showing systematic vs. random structure. (d) Diagnostic decision tree for failure mode identification.

2.9.5 Diagnostic Decision Tree

Design Rule: Failure Mode Diagnostic Protocol

When QFI reconstruction quality is unsatisfactory, follow this decision tree:

Step 1: Check measurement quality

- Is $\sigma_F < 2 \times \sigma_F^{\text{QPN}}$? If no → Level 1 failure (measurement)

Step 2: Check conditioning

- Is $\kappa < 100 \times \text{SNR}$? If no → Level 2 failure (conditioning)
- Is $\Gamma_{\text{inv}} > 0.5$? If no → add physics channels or increase regularization

Step 3: Check model accuracy

- Is $\chi^2/N_{\text{dof}} < 2$? If no → Level 3 failure (model mismatch)
- Are residuals white (no patterns)? If no → systematic model error

Step 4: If all checks pass but results unsatisfactory

- Problem may be intrinsically difficult (source at depth limit)
- Consider if QFI is appropriate for this application

2.9.6 Preventive Measures

Failure Mode	Preventive Measure	Monitoring Metric
Low SNR	Regular laser/optics maintenance	σ_F tracking
Poor conditioning	Multi-physics by default	κ computation
Model mismatch	Periodic calibration	Residual χ^2
Depth ambiguity	Include thermal channel	CRB correlation
Drift	Temperature stabilization	Long-term σ_F trend

Table 2.17: Preventive measures for common failure modes

2.10 Complete Uncertainty Propagation Chain

2.10.1 From Photon Shot Noise to Source Confidence Intervals

The complete uncertainty propagation chain traces noise from its physical origin (photon shot noise) through measurement, reconstruction, and final source parameter uncertainty.

Key Equation: Complete Uncertainty Chain

$$\sigma_S = \underbrace{\frac{1}{C\gamma\sqrt{N\eta T_2^*}}}_{\text{QPN: } \sigma_F} \times \underbrace{\sqrt{\kappa^2/\text{SNR}^2}}_{\text{Conditioning: } 1/\sqrt{\Gamma_{\text{inv}}}} \times \underbrace{\frac{1}{\sqrt{\Gamma_{\text{mm}}}}}_{\text{Model}} \quad (2.90)$$

2.10.2 Uncertainty Budget Table

Stage	Contribution	Typical Value	Cumulative
Photon shot noise	σ_{photon}	1 (reference)	1.0
QPN limit	$\sigma_F/\sigma_{\text{photon}}$	1.2	1.2
Technical noise	Additional floor	1.1	1.3
Conditioning (Γ_{inv})	$1/\sqrt{\Gamma_{\text{inv}}}$	1.2 ($\Gamma_{\text{inv}} = 0.7$)	1.6
Model mismatch (Γ_{mm})	$1/\sqrt{\Gamma_{\text{mm}}}$	1.05 ($\Gamma_{\text{mm}} = 0.9$)	1.7
Total		1.7×	

Table 2.18: Uncertainty budget for typical QFI system

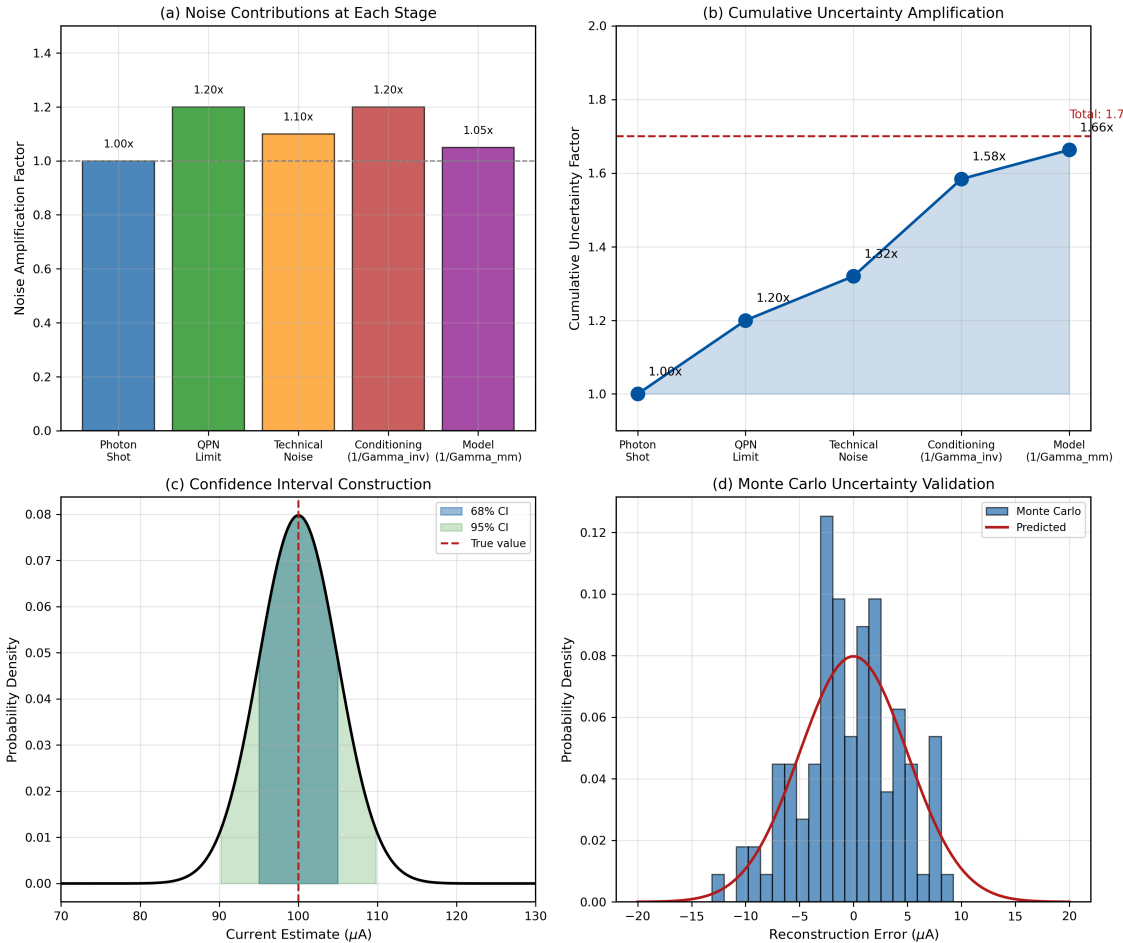


Figure 2.9: Complete uncertainty propagation chain. (a) Noise sources at each stage of the QFI pipeline. (b) Cumulative uncertainty amplification. (c) Confidence interval construction for source parameters. (d) Monte Carlo validation of uncertainty estimates.

2.10.3 Confidence Interval Construction

For Gaussian uncertainties, confidence intervals are:

$$68\% \text{ CI} : \hat{S} \pm \sigma_S \quad (2.91)$$

$$95\% \text{ CI} : \hat{S} \pm 1.96\sigma_S \quad (2.92)$$

$$99\% \text{ CI} : \hat{S} \pm 2.58\sigma_S \quad (2.93)$$

For non-Gaussian posteriors (common in ill-conditioned problems), use percentile-based intervals from MCMC or bootstrap sampling.

2.11 Global Shutter Design Rules for Dynamic QFI

2.11.1 Rolling vs. Global Shutter: Fundamental Distinction

For QFI of dynamic phenomena, the readout mode determines whether spatial correlations in the measured field represent a true instantaneous snapshot.

Aspect	Rolling Shutter	Global Shutter
Exposure	Sequential row-by-row	Simultaneous all pixels
Temporal skew	$\Delta t = N_{\text{rows}} \times t_{\text{row}}$	$\Delta t = 0$ (instantaneous)
Spatial correlation	Time-smeared (corrupted)	True snapshot (preserved)
Dynamic QFI	Invalid for $v > \delta x / \Delta t$	Always valid
Typical sensors	Most sCMOS	Global shutter sCMOS

Table 2.19: Rolling vs. global shutter comparison for QFI

Design Rule: Global Shutter Requirement

Mandatory condition: Use global shutter when:

$$v_{\text{feature}} \times t_{\text{rolling}} > \frac{\delta x_{\text{target}}}{3} \quad (2.94)$$

Practical guidelines:

- Magnetic domain walls ($v \sim 100$ m/s): Global shutter required
- Thermal transients ($\tau \sim 1$ ms): Global shutter recommended
- Static defects: Rolling shutter acceptable

Frame rate consideration: Global shutter typically reduces maximum frame rate by 2–3× compared to rolling shutter. Budget accordingly.

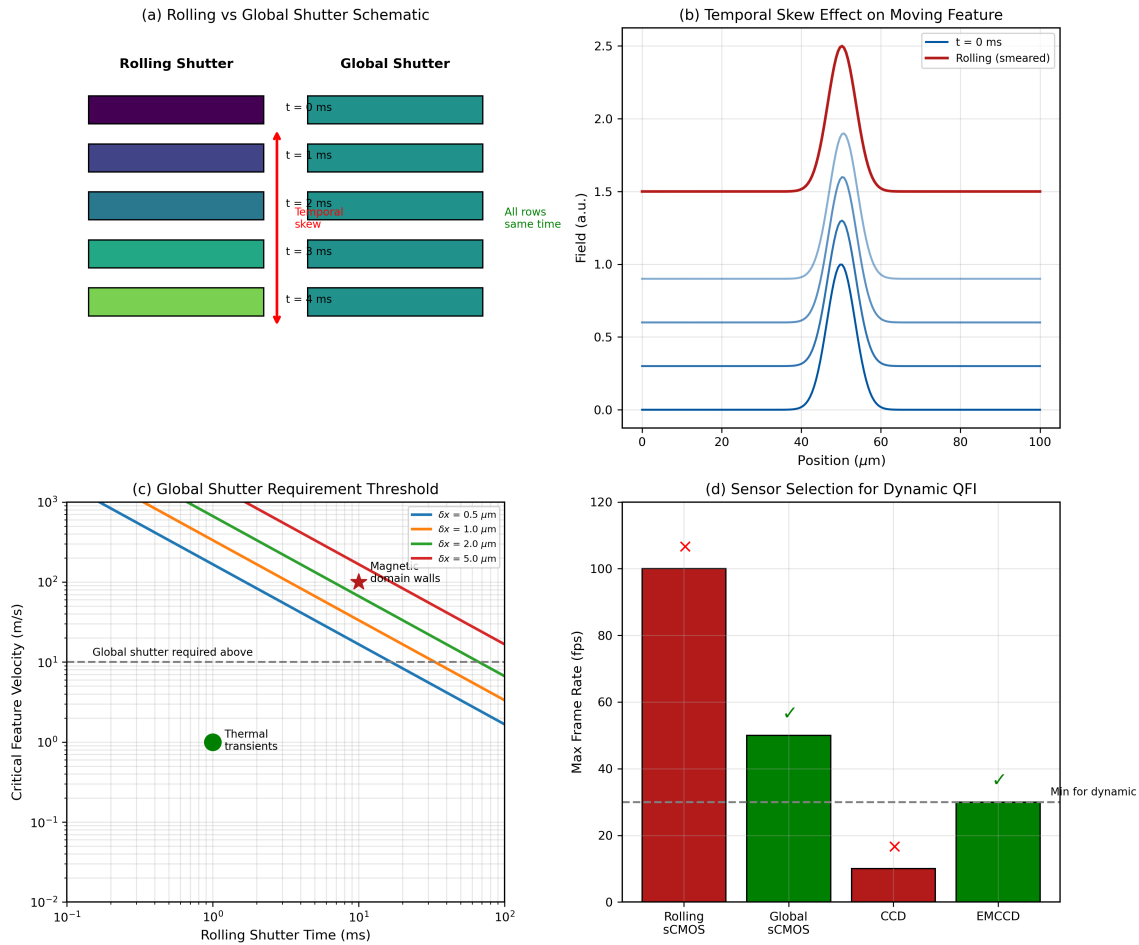


Figure 2.10: Global shutter requirement for dynamic QFI. (a) Schematic comparison of rolling vs. global shutter readout. (b) Temporal skew effect on field correlation. (c) Critical velocity threshold vs. frame time. (d) Recommended sensor selection chart.

2.12 Consolidated Design Rules

This section consolidates all design rules from Chapter 2 for quick reference.

DR #	Title	Specification	Section
2.1	Global Shutter for Dynamic QFI	Required when $v \cdot t_{\text{roll}} > \delta x / 3$	2.1
2.2	QPN Design Targets	$N > 10^5$, $C > 0.25$, $\eta > 0.1$, $T_2^* > 1 \mu\text{s}$ for sub-nT	2.2
2.3	Single-Physics Resolution	$\text{SNR} > (z/\delta x)^2$ required	2.4
2.4	CRB Benchmark	Target $\Gamma_{\text{inv}} > 0.7$ for production	2.5
2.5	Γ_{inv} Design Targets	Multi-physics when $\kappa > 100 \times$ SNR	2.6
2.6	Γ_{mm} Design Targets	$\Gamma_{\text{mm}} > 0.9$, no $\epsilon > 0.15$	2.7
2.7	Multi-Physics Selection	Prioritize complementary depth dependence	2.8
2.8	Diagnostic Protocol	Three-level check: SNR, κ , χ^2	2.9

Table 2.20: Consolidated design rules from Chapter 2

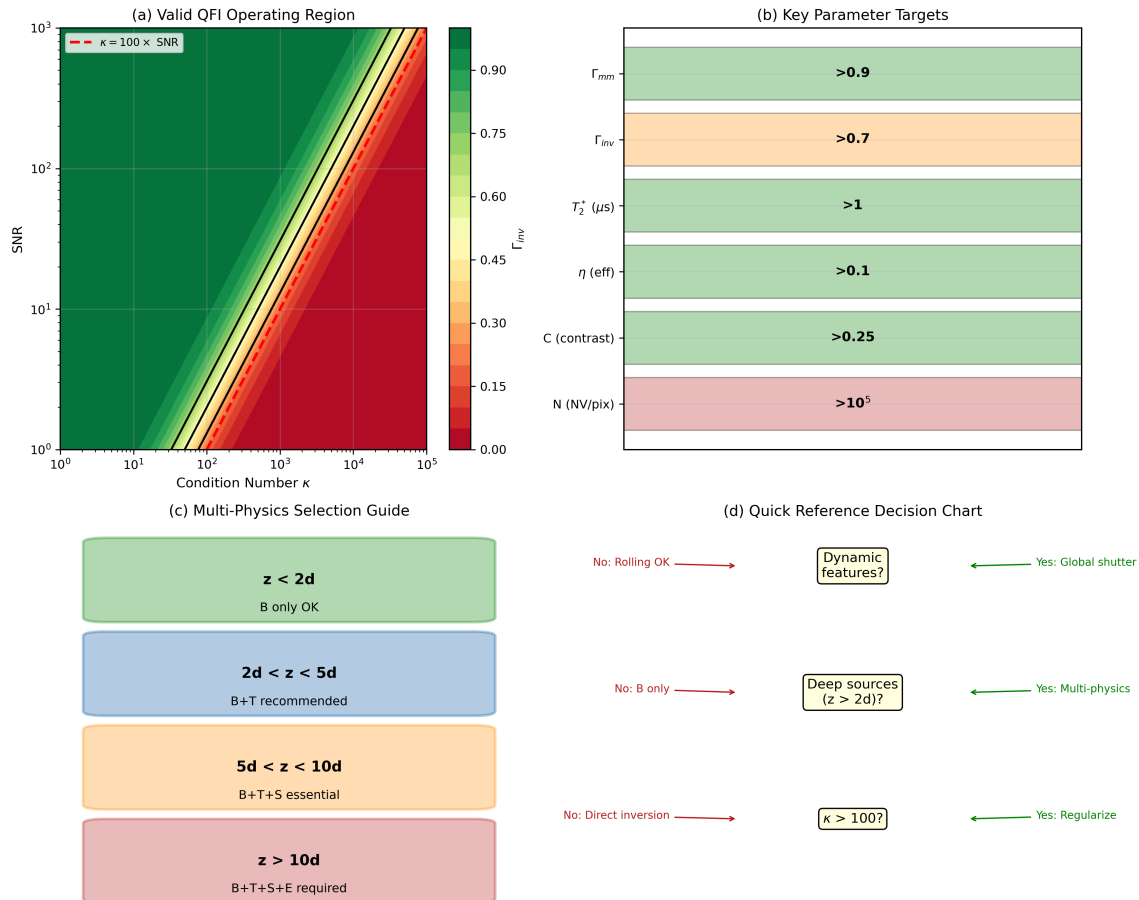


Figure 2.11: Design rules summary visualization. (a) Operating regime map showing valid QFI region. (b) Parameter targets overview. (c) Multi-physics selection guide. (d) Quick reference decision chart.

2.13 Verification Workflow

2.13.1 QFI System Qualification Protocol

Every QFI system should undergo systematic verification before deployment:

1. Measurement verification (Level 1)

- Measure σ_F and compare to QPN limit
- Verify SNR meets specification
- Check spatial resolution via MTF

2. Reconstruction verification (Level 2)

- Compute κ of forward model
- Run synthetic reconstruction tests
- Verify $\Gamma_{inv} > 0.7$ target

3. Calibration verification (Level 3)

- Measure residuals on calibration targets
- Verify $\Gamma_{mm} > 0.9$

- Check for systematic patterns

4. End-to-end validation

- Test on known sources
- Verify uncertainty estimates via repeated measurements
- Document Q_{IFOM} achieved

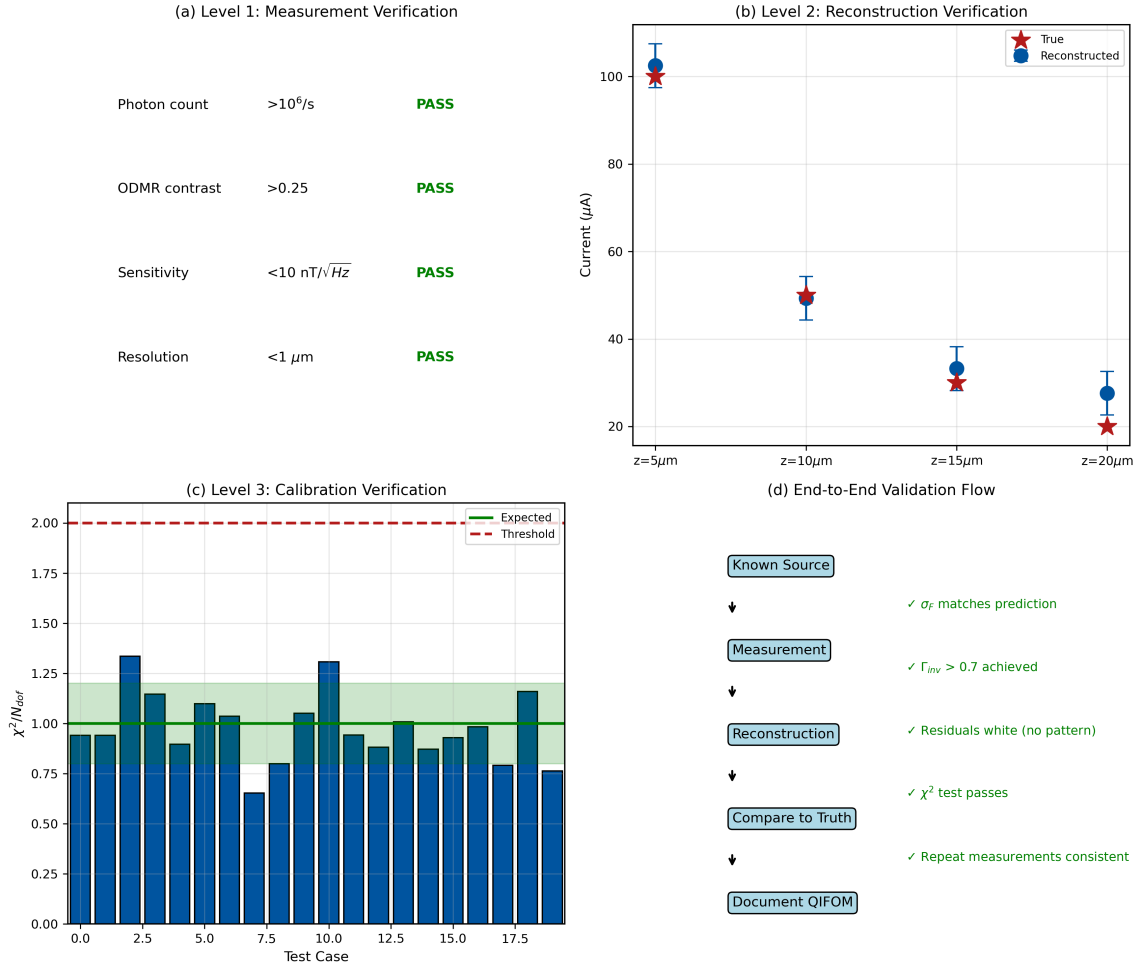


Figure 2.12: QFI verification workflow. (a) Level 1: measurement qualification. (b) Level 2: reconstruction testing with synthetics. (c) Level 3: calibration verification. (d) End-to-end validation flowchart.

2.14 Chapter Summary

2.14.1 Three-Level Framework Recap

Level	Limit	Key Equation	Metric
1: Measurement	Quantum projection noise	$\sigma_B \propto 1/\sqrt{NT_2^*}$	Q_{FOM}
2: Reconstruction	Cramér-Rao bound	$\sigma_S \geq \sqrt{\text{CRB}}$	Γ_{inv}
3: System	Model-mismatch	$\Gamma_{\text{mm}} = \prod(1 - \epsilon_i^2)$	Γ_{mm}

Table 2.21: Three-level limit framework summary

2.14.2 Key Theorems

Theorem	Statement	Implication
2.1 (QPN Limit)	$\delta B \propto 1/\sqrt{N\eta t}$	Detection floor
2.2 (Trade-off)	$\delta B \cdot \delta x \geq K$	Trade-off conserved
2.3 (Depth)	$\delta x_{\min} = z/\sqrt{\text{SNR}}$	Baseline constraint
2.4 (CRB)	$\sigma_S \geq \sqrt{\mathbf{J}^{-1}}$	Reconstruction floor
2.5 (Multi-physics)	$\kappa_{\text{multi}} < \kappa_{\text{single}}$	Extended capability

Table 2.22: Key theorems of Chapter 2

2.14.3 Central Message

The Central Message of Chapter 2

Fundamental limits exist at three levels: measurement, reconstruction, and system. While measurement limits (Level 1) are set by physics, reconstruction limits (Level 2) can be extended through multi-physics correlation, which improves both information content (Φ_{multi}) and conditioning (Γ_{inv}). System limits (Level 3) require careful calibration to maintain $\Gamma_{\text{mm}} > 0.9$.

The complete QFI figure of merit is:

$$Q_{\text{IFOM}} = Q_{\text{FOM}} \times \Gamma_{\text{inv}} \times \Gamma_{\text{mm}} \quad (2.95)$$

Optimizing only Q_{FOM} without considering Γ_{inv} and Γ_{mm} yields a fast but unreliable imager. True QFI excellence requires all three factors.

Problems and Solution Hints

Problem 2.1: QPN Limit Derivation

Derive the Quantum Projection Noise limit for an ensemble of N NV centers with readout contrast C and collection efficiency η .

Given: NV ensemble with $N = 10^4$ centers, $C = 0.3$, $\eta = 0.1$, $T_2^* = 1 \mu\text{s}$, $\gamma = 28 \text{ GHz/T}$.

Find:

- (a) Derive the expression for magnetic field sensitivity σ_B^{QPN} .
- (b) Calculate the numerical sensitivity in $\text{nT}/\sqrt{\text{Hz}}$.
- (c) How does sensitivity scale if you double N ? Double T_2^* ?

Hint: Start from the binomial statistics of spin projection measurements. At optimal working point ($\theta = \pi/2$), the probability is $p = 1/2$ and variance is $N/4$.

Problem 2.2: Resolution-Sensitivity Trade-off

A QFI system must image features at $\delta x = 0.5 \mu\text{m}$ resolution with sensitivity $\sigma_B < 5 \text{ nT}/\sqrt{\text{Hz}}$.

Given: NV density $\rho_{\text{NV}} = 10^{17} \text{ cm}^{-3}$, layer thickness $d = 100 \text{ nm}$, $C = 0.3$, $\eta = 0.1$, $T_2^* = 1 \mu\text{s}$.

Find:

- (a) Calculate the trade-off constant K .
- (b) Is the target ($\delta x = 0.5 \mu\text{m}$, $\sigma_B < 5 \text{ nT}$) achievable?
- (c) What NV density would be needed to achieve both targets?

Hint: Use the trade-off equation $\sigma_B \cdot \delta x = K$ and solve for requirements.

Problem 2.3: Depth Limit Analysis

A buried current at depth $z = 30 \mu\text{m}$ must be imaged with $\delta x = 3 \mu\text{m}$ resolution using magnetic-only QFI.

Given: Standoff distance $d = 5 \mu\text{m}$, pixel size $\Delta x = 1 \mu\text{m}$.

Find:

- (a) What SNR is required according to the depth theorem?
- (b) Calculate the condition number κ of the forward model.
- (c) Is this reconstruction practically achievable with single-physics? Justify quantitatively.

Hint: Apply both the depth theorem ($\delta x_{\min} = z/\sqrt{\text{SNR}}$) and condition number scaling ($\kappa = e^{\pi z/\Delta x}$).

Problem 2.4: Cramér-Rao Bound Calculation

For a point current source with parameters $\mathbf{S} = (I, z)^T$, compute the CRB for both parameters.

Given: Measurement at $N = 100$ pixels over $100 \times 100 \mu\text{m}^2$ FOV, $\sigma_B = 10 \text{ nT}$, source at $I = 100 \mu\text{A}$, $z = 10 \mu\text{m}$.

Find:

- (a) Write the forward model $B(x; I, z)$ for a line current.
- (b) Calculate the Jacobian matrix elements $\partial B / \partial I$ and $\partial B / \partial z$.
- (c) Compute the Fisher Information Matrix \mathbf{J} .
- (d) What is the CRB for I and z ? What is their correlation?

Hint: The magnetic field from a line current at depth z is $B(x) = \mu_0 I z / [2\pi(x^2 + z^2)]$.

Problem 2.5: Γ_{inv} and Multi-Physics Improvement

Compare reconstruction fidelity for single-physics vs. multi-physics QFI.

Given: Forward model condition numbers $\kappa_B = 1000$ (magnetic only), $\kappa_{B+T} = 100$ (magnetic + thermal), SNR = 100, $\kappa_0 = 50$.

Find:

- (a) Calculate Γ_{inv} for single-physics using the proxy formula.
- (b) Calculate Γ_{inv} for multi-physics.
- (c) What is the improvement factor?
- (d) At what depth does single-physics achieve $\Gamma_{\text{inv}} = 0.5$?

Hint: Use $\Gamma_{\text{inv}} \approx 1/[1 + (\kappa/\kappa_0)^2/\text{SNR}^2]$.

Problem 2.6: Model-Mismatch Budget

Design an error budget to achieve $\Gamma_{\text{mm}} > 0.9$ for a production QFI system.

Given: Potential error sources with maximum ϵ values: standoff (15%), PSF (10%), MW field (8%), tilt (5%), temperature (3%).

Find:

- (a) Calculate Γ_{mm} if all errors are at maximum.
- (b) Which single error source has the largest impact?
- (c) Design calibration targets to achieve $\Gamma_{\text{mm}} > 0.9$.
- (d) How much can standoff error increase if PSF is calibrated to 3%?

Hint: Use $\Gamma_{\text{mm}} = \prod(1 - \epsilon_i^2)$ and sensitivity analysis.

Problem 2.7: Complete Q_{IFOM} Optimization

Optimize the complete QFI figure of merit for a semiconductor FA application.

Given: Current system: $N_{\text{NV}} = 10^5/\text{pixel}$, $t_{\text{acq}} = 2 \text{ s}$, SNR = 50, $\Gamma_{\text{inv}} = 0.4$, $\Gamma_{\text{mm}} = 0.85$.

Find:

- (a) Calculate current Q_{FOM} and Q_{IFOM} .
- (b) Which single factor improvement would have the largest impact?
- (c) If adding thermal sensing improves Γ_{inv} to 0.7 but increases t_{acq} to 3 s, is it worthwhile?
- (d) Design a roadmap to double Q_{IFOM} .

Hint: $Q_{\text{IFOM}} = (N/t) \times \text{SNR}^2 \times \Gamma_{\text{inv}} \times \Gamma_{\text{mm}}$.

Problem 2.8: Global Shutter Requirement

Determine whether global shutter is required for a specific QFI application.

Given: Imaging magnetic domain walls moving at $v = 50 \text{ m/s}$ with $\delta x = 2 \mu\text{m}$ target resolution. Camera options: rolling shutter (sweep time 10 ms) or global shutter (max frame rate 50 fps).

Find:

- (a) Calculate the displacement during rolling shutter sweep.
- (b) Apply the global shutter criterion (Equation 2.1).

- (c) What is the maximum velocity that rolling shutter can handle?
- (d) Recommend a camera choice with justification.

Hint: Global shutter required when $v \cdot t_{\text{roll}} > \delta x/3$.

Problem 2.9: Failure Mode Diagnosis

A QFI system shows unexpectedly large reconstruction errors. Diagnose the failure mode using the three-level framework.

Given: Measured $\sigma_F = 8 \text{ nT}$ (expected QPN: 5 nT), reconstruction MSE = $50 \mu\text{A}^2$ (expected CRB: $10 \mu\text{A}^2$), residual $\chi^2/N_{\text{dof}} = 3.5$.

Find:

- (a) Check Level 1: Is $\sigma_F < 2 \times \sigma_F^{\text{QPN}}$?
- (b) Check Level 2: What Γ_{inv} is implied by MSE/CRB?
- (c) Check Level 3: Does χ^2 indicate model mismatch?
- (d) Identify the primary failure mode and recommend remediation.

Hint: Apply the diagnostic decision tree systematically.

Problem 2.10: Multi-Physics Conditioning Theorem

Prove that multi-physics measurement improves forward model conditioning.

Given: Single-physics forward model \mathbf{G}_B with singular values $\sigma_1^B > \sigma_2^B > \dots > \sigma_n^B$. Adding thermal physics gives stacked model $\mathbf{G}_{\text{multi}} = [\mathbf{G}_B^T, \mathbf{G}_T^T]^T$.

Find:

- (a) Show that $\mathbf{J}_{\text{multi}} = \mathbf{J}_B + \mathbf{J}_T$.
- (b) Prove that $\lambda_{\min}(\mathbf{J}_{\text{multi}}) \geq \lambda_{\min}(\mathbf{J}_B)$.
- (c) Under what condition does $\kappa_{\text{multi}} < \kappa_B$?
- (d) Explain physically why magnetic and thermal provide complementary information for depth estimation.

Hint: Use the SVD relationship between singular values and FIM eigenvalues.

References

- [2.1] Degen, C. L., Reinhard, F., & Cappellaro, P. (2017). Quantum sensing. *Reviews of Modern Physics*, 89(3), 035002.
- [2.2] Taylor, J. M., et al. (2008). High-sensitivity diamond magnetometer with nanoscale resolution. *Nature Physics*, 4(10), 810–816.
- [2.3] Rondin, L., et al. (2014). Magnetometry with nitrogen-vacancy defects in diamond. *Reports on Progress in Physics*, 77(5), 056503.
- [2.4] Barry, J. F., et al. (2020). Sensitivity optimization for NV-diamond magnetometry. *Reviews of Modern Physics*, 92(1), 015004.
- [2.5] Pham, L. M., et al. (2011). Magnetic field imaging with nitrogen-vacancy ensembles. *New Journal of Physics*, 13(4), 045021.
- [2.6] Broadway, D. A., et al. (2018). Spatial mapping of band bending in semiconductor devices using in situ quantum sensors. *Nature Electronics*, 1(9), 502–507.
- [2.7] Tetienne, J.-P., et al. (2017). Quantum imaging of current flow in graphene. *Science Advances*, 3(4), e1602429.
- [2.8] Van Trees, H. L. (2001). *Detection, Estimation, and Modulation Theory, Part I*. John Wiley & Sons.
- [2.9] Kay, S. M. (1993). *Fundamentals of Statistical Signal Processing: Estimation Theory*. Prentice Hall.
- [2.10] Hansen, P. C. (1998). *Rank-Deficient and Discrete Ill-Posed Problems: Numerical Aspects of Linear Inversion*. SIAM.
- [2.11] Vogel, C. R. (2002). *Computational Methods for Inverse Problems*. SIAM.
- [2.12] Engl, H. W., Hanke, M., & Neubauer, A. (1996). *Regularization of Inverse Problems*. Springer.
- [2.13] Kucska, G., et al. (2013). Nanometre-scale thermometry in a living cell. *Nature*, 500(7460), 54–58.
- [2.14] Neumann, P., et al. (2013). High-precision nanoscale temperature sensing using single defects in diamond. *Nano Letters*, 13(6), 2738–2742.
- [2.15] Clevenson, H., et al. (2015). Broadband magnetometry and temperature sensing with a light-trapping diamond waveguide. *Nature Physics*, 11(5), 393–397.
- [2.16] Glenn, D. R., et al. (2015). Single-cell magnetic imaging using a quantum diamond microscope. *Nature Methods*, 12(8), 736–738.
- [2.17] Le Sage, D., et al. (2013). Optical magnetic imaging of living cells. *Nature*, 496(7446), 486–489.
- [2.18] Jakobi, I., et al. (2017). Measuring broadband magnetic fields on the nanoscale using a hybrid quantum register. *Nature Nanotechnology*, 12(1), 67–72.
- [2.19] Steinert, S., et al. (2013). Magnetic spin imaging under ambient conditions with sub-cellular resolution. *Nature Communications*, 4(1), 1607.
- [2.20] Simpson, D. A., et al. (2017). Non-neurotoxic nanodiamond probes for intraneuronal temperature mapping. *ACS Nano*, 11(12), 12077–12086.